Eur. Phys. J. C 14, 347–365 (2000)
Digital Object Identifier (DOI) 10.1007/s100520000333

THE EUROPEAN PHYSICAL JOURNAL C

Stability of the lepton-flavor mixing matrix against quantum corrections

N. Haba[1,2,a], N. Okamura[3,b]

[1] Department of Physics, The Ohio State University, Columbus, OH 43210, USA
[2] Faculty of Engineering, Mie University, Tsu Mie 514-8507, Japan
[3] Theory Group, KEK, Tsukuba Ibaraki 305-0801, Japan

Received: 24 June 1999 / Revised version: 23 December 1999 /
Published online: 17 March 2000 – © Springer-Verlag 2000

Abstract. Recent neutrino experiments suggest strong evidence of tiny neutrino masses and the lepton-flavor mixing. Neutrino-oscillation solutions for the atmospheric neutrino anomaly and the solar neutrino deficit can determine the texture of the neutrino mass matrix according to the neutrino mass hierarchies as Type A: $m_3 \gg m_2 \sim m_1$, Type B: $m_3 \ll m_2 \sim m_1$, and Type C: $m_3 \sim m_2 \sim m_1$, where m_i is the i-th generation neutrino mass. In this paper we study the stability of the lepton-flavor mixing matrix against quantum corrections for all three types of mass hierarchy in the minimal supersymmetric Standard Model with an effective dimension-five operator which gives the Majorana masses of neutrinos. The relative sign assignments of neutrino masses in each type play crucial role for the stability against quantum corrections. We find that the lepton-flavor mixing matrix of Type A is stable against quantum corrections, and that of Type B with the same (opposite) signs of m_1 and m_2 are unstable (stable). For Type C, the lepton-flavor-mixing matrix approaches the definite unitary matrix according to the relative sign assignments of the neutrino mass eigenvalues as the effects of quantum corrections become large enough to neglect the squared mass differences of neutrinos.

1 Introduction

Recent neutrino experiments suggest strong evidence of tiny neutrino masses and flavor mixing in the lepton sector [1]-[4]. Studies of the lepton-flavor-mixing matrix, which we call the Maki-Nakagawa-Sakata (MNS) [5] matrix, point to new steps of flavor physics. Especially, the study of the energy-scale dependence of the MNS matrix is one of the main issues to investigate new physics beyond the Standard Model (SM) [6].

There following neutrino-oscillation solutions exist for the solar neutrino deficit and the atmospheric neutrino anomaly:

$$\Delta m^2_{\rm solar} \sim \begin{cases} 0.85\times 10^{-10}\ {\rm eV}^2 \\ \quad \text{(vacuum solution)}, \\ 1.8\times 10^{-5}\ {\rm eV}^2 \\ \quad \text{(MSW-large mixing solution)}, \\ 0.8\times 10^{-5}\ {\rm eV}^2 \\ \quad \text{(MSW-small mixing solution)}, \end{cases} \tag{1.1a}$$

$$\Delta m^2_{\rm ATM} \sim 3.7\times 10^{-3}\ \ {\rm eV}^2\,, \tag{1.1b}$$

where $\Delta m^2_{\rm solar}$ and $\Delta m^2_{\rm ATM}$ stand for the squared mass differences of the solar neutrino deficit [1] and the atmospheric neutrino anomaly [2,3], respectively. In this article, we adopt the scenario of three-generation neutrinos, which implies

$$\begin{aligned} \Delta m^2_{\rm solar} &\equiv \left| m_2^2 - m_1^2 \right|\,, \quad \text{and} \\ \Delta m^2_{\rm ATM} &\equiv \left| m_3^2 - m_2^2 \right|\,, \end{aligned} \tag{1.2}$$

where m_i is the i-th ($i = 1 \sim 3$) generation neutrino mass ($m_i \geq 0$). We take the following typical values of the mixing angles in each solution:

$$\sin^2 2\theta_{\rm solar} = \begin{cases} 1 \\ \quad \text{(vacuum solution)}, \\ 1 \\ \quad \text{(MSW-large mixing solution)}, \\ 0.017 \\ \quad \text{(MSW-small mixing solution)}, \end{cases} \tag{1.3a}$$

$$\sin^2 2\theta_{\rm ATM} = 1 \ \text{(atmospheric neutrino anomaly)} \tag{1.3b}$$

$$\sin^2 2\theta_{\rm CHOOZ} = 0 \ \text{(CHOOZ experiment)}\,. \tag{1.3c}$$

Under the assignments of (1.2), there are the following three possible types of neutrino mass hierarchy [7];

$$\text{Type A} \ : \ m_1 \sim m_2 \ll m_3\,, \tag{1.4a}$$

[a] e-mail: haba@pacific.mps.ohio-state.edu
[b] e-mail: naotoshi.okamura@kek.jp

$$\text{Type B} \ : \ m_1 \sim m_2 \gg m_3 \,, \tag{1.4b}$$
$$\text{Type C} \ : \ m_1 \sim m_2 \sim m_3 \,. \tag{1.4c}$$

In this article we study the stability of the MNS matrix for these three types of neutrino mass hierarchy against quantum corrections in the minimal supersymmetric Standard Model (MSSM) with the effective dimension-five operator which gives the Majorana masses of neutrinos. Since the negative sign assignments of m_i in (1.4) also satisfy (1.2), we consider all relative sign assignments for the masses in each type. We determine the MNS matrix elements at the low-energy scale from the neutrino-oscillation experiments, and analyze whether the MNS matrix is stable against quantum corrections in each type of neutrino-mass hierarchy. The results of our analyses are found to depend strongly on the types of neutrino-mass hierarchy and on the relative sign assignments of masses. Our findings are summarized as follows.

Type A: The MNS matrix is stable against quantum corrections.
Type B: The MNS matrix is stable when m_1 and m_2 have the opposite signs, while it is unstable when m_1 and m_2 have the same signs.
Type C: The MNS matrix approaches a definite unitary matrix according to the relative sign assignments of the neutrino masses, as the effects of quantum corrections become large enough to neglect any squared masse differences of the neutrino.

Our results are consistent with those of the recent works [8]-[10] which studied the related subject for certain specific cases. In the case of Type C for the relative sign assignments $(m_1, -m_2, m_3)$, where each m_i is non-negative, the relation between the eigenvectors at the m_Z scale and that at the M_R scale found in [8] for large $\tan\beta$ is consistent with ours. Also in the case of Type C with the eigenvalues as $(-m_1, m_2, m_3)$, the result of [9] is consistent with ours. When the present work has been essentially completed, we received the work of [10], which studies the case of Type B. Our results agree with theirs. We believe that our comprehensive study will serve as a clue of the flavor physics.

This article is organized as follows. In Sect. 2, we determine the elements of the MNS matrix from the data of recent neutrino-oscillation experiments. In Sect. 3, we estimate the magnitude of quantum corrections of the dimension-five Majorana operator. In Sect. 4, we study the stability of the MNS matrix against renormalization effects in the two-generation case. In Sect. 5, we analyze the stability of the MNS matrix against quantum corrections in the three-generation case for each type of mass hierarchy. Section 6 gives our conclusions.

2 The Maki-Nakagawa-Sakata matrix

In this section, we give a definition and parameterization [11] of the Maki-Nakagawa-Sakata (MNS) lepton-flavor mixing matrix [5]. We determine elements of the MNS matrix from the data of recent neutrino-oscillation experiments [1]-[4].

2.1 Definition

The effective Yukawa Lagrangian in the lepton sector is given by

$$\mathcal{L}^{\rm low}_{yukawa} = {y^{\rm e}}_{ij}\phi_{\rm d} L_i \cdot e^c_{Rj} - \frac{1}{2}\kappa_{ij}(\phi_{\rm u} L_i)\cdot(\phi_{\rm u} L_j) + h.c.\,, \tag{2.1}$$

where $y^{\rm e}$ is the Yukawa matrix of the charged lepton. $\phi_{\rm u}$ and $\phi_{\rm d}$ are the $SU(2)_L$ doublet Higgs bosons that give Dirac masses to the up-type and down-type fermions, respectively. L_i is the i-th generation $SU(2)_L$ doublet lepton. e_{Ri} is the i-th generation charged lepton. The matrix κ induces the neutrino Majorana mass matrix, which is complex and symmetric.

We now give a definition of the 3×3 MNS matrix, which is defined analogously to the CKM matrix [12,13]. Unitary matrices of $U_{\rm e}$ and U_ν transform the mass-eigenstates into the weak-current eigenstates as

$$\begin{pmatrix} l_{L1} \\ l_{L2} \\ l_{L2} \end{pmatrix} = U_{\rm e} \begin{pmatrix} e_L \\ \mu_L \\ \tau_L \end{pmatrix}, \qquad \begin{pmatrix} \nu_{L1} \\ \nu_{L2} \\ \nu_{L3} \end{pmatrix} = U_\nu \begin{pmatrix} \nu_1 \\ \nu_2 \\ \nu_3 \end{pmatrix}. \tag{2.2}$$

The MNS matrix is then defined as

$$(V_{\rm MNS})_{\alpha i} \equiv \left(U_{\rm e}^\dagger U_\nu\right)_{\alpha i}\,, \qquad \nu_\alpha = \sum_{i=1}^{3} (V_{\rm MNS})_{\alpha i}\,\nu_i\,, \tag{2.3}$$

where α and i label the neutrino flavors ($\alpha = e, \mu, \tau$) and the mass eigenstates ($i = 1, 2, 3$), respectively.

2.2 Parameterization

The 3×3 MNS matrix generally has three mixing angles and three physical phases for the Majorana neutrinos. We adopt the parameterization [11]

$$V_{\rm MNS} = \underbrace{\begin{pmatrix} U_{e1} & U_{e2} & U_{e3} \\ U_{\mu 1} & U_{\mu 2} & U_{\mu 3} \\ U_{\tau 1} & U_{\tau 2} & U_{\tau 3} \end{pmatrix}}_{U_{\alpha i}} \begin{pmatrix} 1 & 0 & 0 \\ 0 & e^{i\varphi_2} & 0 \\ 0 & 0 & e^{i\varphi_3} \end{pmatrix}. \tag{2.4}$$

The matrix $U_{\alpha i}$, which has three mixing angles and one phase, can be parameterized in the same way as the CKM matrix. Since the data of the present neutrino-oscillation experiments directly constrain elements of U_{e2}, U_{e3}, and $U_{\mu 3}$, the most convenient parameterization is to adopt these three elements as independent parameters [11], analogously to the parameterizations [14,15] at the CKM matrix. Without losing generality, we can take U_{e2} and $U_{\mu 3}$ to be real and non-negative by redefining φ_2 and φ_3. Then,

only U_{e3} has a complex phase. All the other matrix elements can be determined by the unitarity conditions, as follows:

$$\begin{aligned} U_{e1} &= \sqrt{1-|U_{e3}|^2-|U_{e2}|^2}\,, \\ U_{\tau 3} &= \sqrt{1-|U_{e3}|^2-|U_{\mu 3}|^2}\,, \\ U_{\mu 1} &= -\frac{U_{e2}U_{\tau 3}+U_{\mu 3}U_{e1}U_{e3}^*}{1-|U_{e3}|^2}\,, \\ U_{\mu 2} &= \frac{U_{e1}U_{\tau 3}-U_{\mu 3}U_{e2}U_{e3}^*}{1-|U_{e3}|^2}\,, \\ U_{\tau 1} &= \frac{U_{e2}U_{\mu 3}-U_{\tau 3}U_{e1}U_{e3}^*}{1-|U_{e3}|^2}\,, \\ U_{\tau 2} &= -\frac{U_{\mu 3}U_{e1}+U_{e2}U_{\tau 3}U_{e3}^*}{1-|U_{e3}|^2}\,. \end{aligned} \tag{2.5}$$

Here U_{e1} and $U_{\tau 3}$ are chosen real and non-negative, and the other elements are complex.

The relations among the MNS matrix elements and the mixing angles are given by

$$\begin{aligned} &\sin\theta_{13} = |U_{e3}|\,, \quad \sin\theta_{23} = \frac{U_{\mu 3}}{\sqrt{1-|U_{e3}|^2}}\,, \\ &\sin\theta_{12} = \frac{U_{e2}}{\sqrt{1-|U_{e3}|^2}}\,, \end{aligned} \tag{2.6}$$

which can be rewritten as

$$\sin^2 2\theta_{13} = 4|U_{e3}|^2\left(1-|U_{e3}|^2\right)\,, \tag{2.7a}$$

$$\sin^2 2\theta_{23} = 4\frac{U_{\mu 3}^2}{1-|U_{e3}|^2}\left(1-\frac{U_{\mu 3}^2}{1-|U_{e3}|^2}\right)\,, \tag{2.7b}$$

$$\sin^2 2\theta_{12} = 4\frac{U_{e2}^2}{1-|U_{e3}|^2}\left(1-\frac{U_{e2}^2}{1-|U_{e3}|^2}\right)\,, \tag{2.7c}$$

where θ_{ij} is the mixing angle between the i-th and j-th generations. In general, these mixing angles are not the same as those obtained from two-generation analyses of the experimental results.

2.3 The MNS matrix at the weak scale

Now let us fix constrain the independent parameters of the MNS matrix, U_{e2}, U_{e3} and $U_{\mu 3}$ from the data of neutrino-oscillation experiments.

2.3.1 $|U_{e3}|$

The CHOOZ experiment [4] measures the survival probability of $\overline{\nu_e}$. The result of this experiment shows that

$$\sin^2 2\theta_{\rm CHOOZ} < 0.18\,, \quad \text{for} \quad \delta m^2_{\rm CHOOZ} > 1\times 10^{-3}{\rm eV}^2. \tag{2.8}$$

By using the above result, we can obtain the following constraint:

$$|U_{e3}|^2\left(1-|U_{e3}|^2\right) < 0.045\,, \tag{2.9a}$$

$$\text{for} \quad |m_3^2-m_1^2| \simeq |m_3^2-m_2^2| > 1\times 10^{-3}{\rm eV}^2\,. \tag{2.9b}$$

In this article we assume the (1,3) element of the MNS matrix at the weak scale m_Z to be

$$U_{e3} = 0\,, \tag{2.10}$$

for brevity.

2.3.2 $U_{\mu 3}$

The atmospheric neutrino data [2,3] suggest the maximal mixing of $\nu_\mu \to \nu_X$ ($\nu_X \neq \nu_\mu, \nu_e$) oscillation[1]. In the three-flavor analysis, the most favorable interpretation of the data is the $\nu_\mu \to \nu_\tau$ oscillation. From (2.7b) and (2.10), we can obtain

$$\sin^2 2\theta_{\rm ATM} = 4U_{\mu 3}^2\left(1-U_{\mu 3}^2\right)\,. \tag{2.11}$$

Thus, by using (1.3b) we fix the (2,3) element of the MNS matrix at the m_Z scale as

$$U_{\mu 3} = \frac{1}{\sqrt{2}}\,. \tag{2.12}$$

2.3.3 U_{e2}

Deficits of solar neutrinos observed at several telestial experiments [1] have been interpreted as $\nu_e \to \nu_X$ ($\nu_X \neq \nu_e\,, \overline{\nu_e}$) oscillation, and the following three solutions are found: the MSW small-mixing solution (MSW-S), the MSW large-mixing solution (MSW-L) [16], and the vacuum-oscillation solution (VO) [17]. By using (2.10), the survival probability of ν_e is simplified as

$$P_{\nu_e\to\nu_e} = 1-4|U_{e1}|^2|U_{e2}|^2\sin^2\left(\frac{\delta m_{12}^2}{4E}L\right)\,. \tag{2.13}$$

Equation (2.10) also simplifies (2.7c) to be

$$\sin^2 2\theta_{\rm SUN} = 4U_{e2}^2\left(1-U_{e2}^2\right)\,. \tag{2.14}$$

Thus, from (1.3a), we determine the value of U_{e2} at the m_Z scale as

$$\begin{aligned} &\text{MSW-S}: U_{e2} = 0.0042\,, \quad \text{MSW-L}: U_{e2} = \frac{1}{\sqrt{2}}\,, \\ &\text{VO}: U_{e2} = \frac{1}{\sqrt{2}}\,, \end{aligned} \tag{2.15}$$

for each solution.

[1] The oscillation of $\nu_\mu \to \nu_e$ is not only disfavored by the CHOOZ experiment data of (2.8), but also disfavored by the Super-Kamiokande data by itself [2,3].

2.3.4 The MNS matrix at the m_Z scale

In this article we neglect the Majorana phases of $\varphi_{2,3}$ in the MNS matrix of (2.4) for simplicity. By using (2.5), (2.10) and (2.12), the MNS matrix at the m_Z scale is determined to be

$$U_{\rm MNS} = \begin{pmatrix} \cos\theta & \sin\theta & 0 \\ \frac{-\sin\theta}{\sqrt{2}} & \frac{\cos\theta}{\sqrt{2}} & \frac{1}{\sqrt{2}} \\ \frac{\sin\theta}{\sqrt{2}} & \frac{-\cos\theta}{\sqrt{2}} & \frac{1}{\sqrt{2}} \end{pmatrix}, \tag{2.16}$$

where the angle θ[2] depends on the solution of the solar neutrino deficits as

$$\sin\theta = \begin{cases} 0.0042 \ (\theta = 0.0042) & \text{(MSW-S)}\,, \\ \frac{1}{\sqrt{2}} \ (\theta = \frac{\pi}{4}) & \text{(MSW-L)}\,, \\ \frac{1}{\sqrt{2}} \ (\theta = \frac{\pi}{4}) & \text{(VO)}\,, \end{cases} \tag{2.17}$$

which are obtained from (2.15).

3 Quantum corrections of κ

The renormalization group equation (RGE) of κ, which is the coefficient of dimension-five operator in the effective Lagrangian of (2.1), has been studied in [18,19]. It is expected that κ is produced by the see-saw mechanism [20] at the high energy-scale, M_R. In the MSSM, κ satisfies the following RGE at the one-loop level [19]:

$$\begin{aligned} 8\pi^2 \frac{d}{dt}\kappa = & \left\{ {\rm tr}\left(3y^{\rm u}y^{\rm u\dagger}\right) - 4\pi\left(3\alpha_2 + \frac{3}{5}\alpha_1\right)\right\}\kappa \\ & + \frac{1}{2}\left\{ \left(y^{\rm e}y^{\rm e\dagger}\right)\kappa + \kappa\left(y^{\rm e}y^{\rm e\dagger}\right)^T \right\}, \end{aligned} \tag{3.1}$$

where $t = \ln\mu$, and μ is the renormalization scale. $y^{\rm u}$ is the up-quark Yukawa matrix. We notice that once $y^{\rm e}$ is taken diagonal at a certain scale, then the diagonality of $y^{\rm e}$ is kept at all energies in the one-loop level. This is because there are no lepton-flavor-mixing terms, except for κ, in the MSSM Lagrangian. In this base κ is diagonalized by the MNS matrix, and (3.1) is simplified to

$$\begin{aligned} 8\pi^2 \frac{d}{dt}\ln\kappa_{ij} = & \ {\rm tr}\left(3y^{\rm u}y^{\rm u\dagger}\right) - 4\pi\left(3\alpha_2 + \frac{3}{5}\alpha_1\right) \\ & + \frac{1}{2}\left(y_i^2 + y_j^2\right), \end{aligned} \tag{3.2}$$

where y_i ($i = 1 \sim 3$) stands for the i-th generation charged-lepton Yukawa coupling.

[2] From now on, θ_{12} is denoted by θ unless we note otherwise explicitly.

The RGE of κ has two important features [21]. One is that none of the phases in κ depend on the energy-scale. The other is that the RGE of κ can be governed by only n_g equations, where n_g stands for the generation number. In the three-generation case ($n_g = 3$), κ can be parameterized as

$$\begin{aligned} \kappa &= \kappa_{33}\begin{pmatrix} r_1 & c_{12}\sqrt{r_1 r_2} & c_{13}\sqrt{r_1} \\ c_{12}\sqrt{r_1 r_2} & r_2 & c_{23}\sqrt{r_2} \\ c_{13}\sqrt{r_1} & c_{23}\sqrt{r_2} & 1 \end{pmatrix}, \\ &= \kappa_{33}\begin{pmatrix} \sqrt{r_1} & 0 & 0 \\ 0 & \sqrt{r_2} & 0 \\ 0 & 0 & 1 \end{pmatrix}\begin{pmatrix} 1 & c_{12} & c_{13} \\ c_{12} & 1 & c_{23} \\ c_{13} & c_{23} & 1 \end{pmatrix} \\ &\quad \times \begin{pmatrix} \sqrt{r_1} & 0 & 0 \\ 0 & \sqrt{r_2} & 0 \\ 0 & 0 & 1 \end{pmatrix}. \end{aligned} \tag{3.3}$$

Here, c_{ij}'s ($i = 1, 2$ and $j = 2, 3$) are defined as

$$c_{ij}^2 \equiv \frac{\kappa_{ij}^2}{\kappa_{ii}\kappa_{jj}}\,, \tag{3.4}$$

which are energy-scale independent complex parameters. r_i's in (3.3) are defined as

$$r_i \equiv \frac{\kappa_{ii}}{\kappa_{33}}\,, \qquad (i = 1, 2)\,, \tag{3.5}$$

which are always taken to be real and non-negative by the redefinitions of the charged-lepton fields. Since the MNS matrix is independent of the overall factor, κ_{33}, only two real parameters, r_1 and r_2, determine the energy-scale dependence of the MNS matrix.

From (3.2), the RGE of r_i is given by

$$\frac{d}{dt}\ln r_i = \frac{d}{dt}\ln\frac{\kappa_{ii}}{\kappa_{33}} = -\frac{1}{8\pi^2}\left(y_\tau^2 - y_i^2\right), \quad (i = 1, 2)\,, \tag{3.6}$$

where $y_\tau = y^{\rm e}{}_{33}$ is the Yukawa coupling of τ. Since the right-hand side of (3.6) is always negative, the value of r_i decreases as the energy-scale increases. Equation (3.6) can be solved as

$$r_i(M_R) = r_i(m_Z)\frac{I_i}{I_\tau}\,, \tag{3.7}$$

where I_i ($i = 1(e), 2(\mu), \tau$) is defined as

$$I_i \equiv \exp\left(\frac{1}{8\pi^2}\int_{\ln m_Z}^{\ln M_R} y_i^2\ dt\right). \tag{3.8}$$

From (3.3) and (3.7), κ at the M_R scale is determined as

$$\begin{aligned} \kappa(M_R) = & \frac{\kappa_{33}(M_R)}{\kappa_{33}(m_Z)}\begin{pmatrix} \sqrt{I_e/I_\tau} & 0 & 0 \\ 0 & \sqrt{I_\mu/I_\tau} & 0 \\ 0 & 0 & 1 \end{pmatrix} \\ & \times\kappa(m_Z)\begin{pmatrix} \sqrt{I_e/I_\tau} & 0 & 0 \\ 0 & \sqrt{I_\mu/I_\tau} & 0 \\ 0 & 0 & 1 \end{pmatrix}. \end{aligned} \tag{3.9}$$

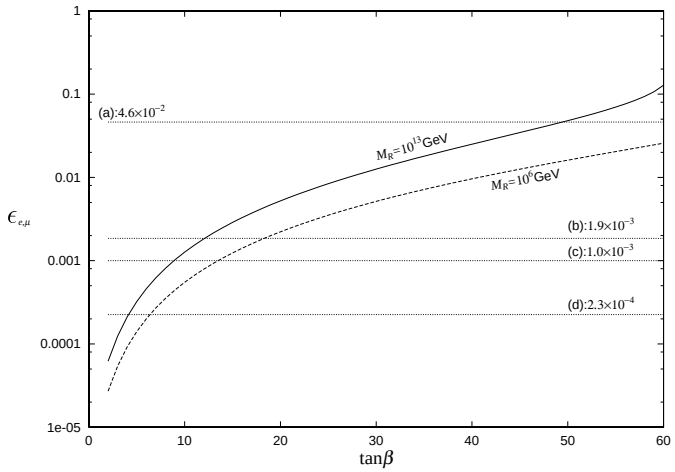

Fig. 1. $\tan\beta$ dependence of $\epsilon_{e,\mu}$. The solid-line (dashed-line) shows $M_R = 10^{13}$GeV (10^6GeV). Each dotted-line shows **a**:4.6×10^{-2}, **b**:1.9×10^{-3}, **c**:1.0×10^{-3} and **d**:2.3×10^{-4}

For completeness, we discuss cases with $\kappa_{33} = 0$ in Appendix A. All the following results are obtained independent of the presence of non-vanishing diagonal elements.

Now let us define the small parameters

$$\epsilon_{e,\mu} = 1 - \sqrt{\frac{I_{e,\mu}}{I_\tau}}\,, \\ = \frac{1}{16\pi^2}\int_{\ln m_Z}^{\ln M_R}\left(y_\tau^2 - y_{e,\mu}^2\right)\,. \qquad (3.10)$$

Figure 1 shows the $\tan\beta(=\langle\phi_{\rm u}\rangle/\langle\phi_{\rm d}\rangle)$ dependences of ϵ_e and ϵ_μ for $M_R = 10^{13}$GeV and 10^6GeV. The magnitudes of $\epsilon_{e,\mu}$ increase as $\tan\beta$ increases, because the quantum correction from τ becomes large in the large $\tan\beta$ region[3]. Since the value of $\sqrt{I_i/I_\tau}$ can be mainly determined by I_τ, the difference of ϵ_e and ϵ_μ is negligible. The solid-line (dashed-line) in Fig. 1 stand for the $\tan\beta$ dependences of $\epsilon_{e,\mu}$ with $M_R = 10^{13}$GeV (10^6GeV). Hereafter, we fix the M_R scale at 10^{13}GeV in our numerical analyses.

4 Two generation case

In this section, we neglect the first-generation contributions for simplicity, and discuss the stability of the MNS matrix against quantum corrections for two-generation neutrinos.

Neglecting the first generation, (3.9) becomes

$$\kappa(M_R) = \frac{\kappa_{33}(M_R)}{\kappa_{33}(m_Z)}\begin{pmatrix}\sqrt{I_\mu/I_\tau} & 0\\ 0 & 1\end{pmatrix} \\ \times\kappa(m_Z)\begin{pmatrix}\sqrt{I_\mu/I_\tau} & 0\\ 0 & 1\end{pmatrix}\,. \qquad (4.1)$$

[3] We show the approximation of $\sqrt{I_i/I_\tau}$ in Appendix B.

We parameterize $\kappa(m_Z)$ as

$$\kappa(m_Z) = \begin{pmatrix}\cos\theta_{23} & \sin\theta_{23}\\ -\sin\theta_{23} & \cos\theta_{23}\end{pmatrix}\begin{pmatrix}\kappa_2 & 0\\ 0 & \kappa_3\end{pmatrix} \\ \times\begin{pmatrix}\cos\theta_{23} & -\sin\theta_{23}\\ \sin\theta_{23} & \cos\theta_{23}\end{pmatrix}\,, \qquad (4.2)$$

where $\kappa_{2,3}$ are the eigenvalues of κ at the m_Z scale. From (4.1), the mixing angle at the M_R scale ($\hat\theta_{23}$) is given by

$$\tan 2\hat\theta_{23} = \frac{\delta_k\sin 2\theta_{23}\,(1-\epsilon)}{\delta\kappa\cos 2\theta_{23} + \epsilon\,(2-\epsilon)\left(\kappa_2 + \delta\kappa\sin^2\theta_{23}\right)}\,, \qquad (4.3)$$

where

$$\epsilon \equiv \epsilon_\mu\,, \quad \text{and} \quad \delta_k \equiv \kappa_3 - \kappa_2\,. \qquad (4.4)$$

Hereafter, we denote the mixing angles at the M_R scale as $\hat\theta_{ij}$'s. Figure 1 shows $0 < \epsilon < 0.15$ for $2 \le \tan\beta \le 60$ with $M_R = 10^{13}$ GeV. We notice that $|\delta_k|$ is not necessarily smaller than $|\kappa_{2,3}|$, because κ_2 can take the opposite sign of κ_3. We classify the neutrino mass hierarchies into the following three cases as Type A$^{(2)}$: $|\kappa_3| \gg |\kappa_2|$, Type B1$^{(2)}$: $\kappa_3 \simeq \kappa_2$ and Type B2$^{(2)}$: $\kappa_3 \simeq -\kappa_2$. We now consider the stability of the mixing angle in each case.

1. Type A$^{(2)}$:
   When $|\kappa_2|$ is much smaller than $|\kappa_3|$ (i.e., $\delta_k \sim |\kappa_3| \gg |\kappa_2| \simeq 0$), (4.2) becomes
   $$\kappa(m_Z) \simeq \kappa_3\,\cos^2\theta_{23}\begin{pmatrix}\tan^2\theta_{23} & \tan\theta_{23}\\ \tan\theta_{23} & 1\end{pmatrix}\,. \qquad (4.5)$$
   In this case, the mixing angle $\hat\theta_{23}$ is given by
   $$\tan 2\hat\theta_{23} = \frac{\sin 2\theta_{23}(1-\epsilon)}{\cos 2\theta_{23} + \epsilon(2-\epsilon)\sin^2\theta_{23}} \\ = \tan 2\theta_{23}\,(1 - \epsilon\sec 2\theta_{23}) + O(\epsilon^2) \qquad (4.6)$$
   from (4.3). This means that $\hat\theta_{23}$ is stable against the quantum correction of ϵ.
2. Type B1$^{(2)}$:
   In the case of $\kappa_2 \simeq \kappa_3$ (i.e., $\kappa_2\kappa_3 > 0,\ 0 < |\delta_k| \ll |\kappa_{2,3}|$), $\kappa(m_Z)$ is given by
   $$\kappa(m_Z) = \begin{pmatrix}\kappa_3 - \delta_k\cos^2\theta_{23} & \delta_k\sin\theta_{23}\cos\theta_{23}\\ \delta_k\sin\theta_{23}\cos\theta_{23} & \kappa_3 - \delta_k\sin^2\theta_{23}\end{pmatrix} \\ \simeq \left(\kappa_3 - \delta_k\sin^2\theta_{23}\right) \\ \times\begin{pmatrix}1 - \dfrac{\delta_k}{\kappa_3}\cos 2\theta_{23} & \dfrac{\delta_k}{2\kappa_3}\sin 2\theta_{23}\\ \dfrac{\delta_k}{2\kappa_3}\sin 2\theta_{23} & 1\end{pmatrix}\,. \qquad (4.7)$$
   Let us discuss the stability of (4.7) against the renormalization effects. Equation (4.3) induces the mixing angle $\hat\theta_{23}$ as
   $$\tan 2\hat\theta_{23} \simeq \frac{\delta_k\sin 2\theta_{23}}{\delta_k\cos 2\theta_{23} + 2\epsilon\kappa_3}\,. \qquad (4.8)$$

Around the maximal mixing at the m_Z scale, $\theta_{23} = \pi/4$, the mixing angle at the M_R scale, $\hat{\theta}_{23}$ becomes

$$\tan 2\hat{\theta}_{23} \simeq \frac{1}{2\epsilon}\,\frac{\delta_k}{\kappa_3}\,, \tag{4.9}$$

This means that the mixing angle $\hat{\theta}_{23}$ strongly depends on the quantum correction ϵ. When the value of δ_k/κ_3 is larger than ϵ, the mixing angle does not receive any significant change from renormalization corrections. On the other hand, when $\epsilon > \delta_k/\kappa_3$, the mixing angle strongly depends on RGE effects, and the mixing angle at the M_R scale can be small even if the maximal mixing is realized at the m_Z scale. This situation has been already discussed in [22].

3. Type $\mathrm{B2}^{(2)}$:
If the absolute value of $\kappa_{2,3}$ is of the same order, but that they have the opposite signs from each other (i.e., $\kappa_2\kappa_3 < 0$, $|\delta_k| \simeq 2|\kappa_{2,3}|$), $\kappa(m_Z)$ is given by

$$\begin{aligned}\kappa(m_Z) &= \kappa_3 \begin{pmatrix} -\cos 2\theta_{23} & \sin 2\theta_{23} \\ \sin 2\theta_{23} & \cos 2\theta_{23} \end{pmatrix} \\ &\quad +\delta_k \begin{pmatrix} \cos^2\theta_{23} & -\sin\theta_{23}\cos\theta_{23} \\ -\sin\theta_{23}\cos\theta_{23} & \sin^2\theta_{23} \end{pmatrix} \\ &\simeq \kappa_3 \cos 2\theta_{23} \begin{pmatrix} -1 & \tan 2\theta_{23} \\ \tan 2\theta_{23} & 1 \end{pmatrix}. \end{aligned} \tag{4.10}$$

In this case, (4.3) induces

$$\begin{aligned}\tan 2\hat{\theta}_{23} &= \tan 2\theta_{23} \left(\frac{2\,(1-\epsilon)}{2-\epsilon\,(2-\epsilon)} \right) \\ &= \tan 2\theta_{23} + O(\epsilon^2)\,. \end{aligned} \tag{4.11}$$

This means that the mixing angle is stable against a small change of ϵ.

Table 1 shows the stability of the MNS matrix against quantum corrections in the two-generation case. The mixing angles of Type $\mathrm{A}^{(2)}$ and Type $\mathrm{B2}^{(2)}$ are stable against a small change of ϵ, implying that they are stable against quantum corrections. The mixing angle of Type $\mathrm{B1}^{(2)}$ is unstable around $\theta_{23} = \pi/4$ when $\epsilon > (\kappa_3 - \kappa_2)/\kappa_3$. When ϵ is bigger than the ratio $(\kappa_3 - \kappa_2)/\kappa_3$, the mixing angle at high energies is very different from that are observed at low energies. Table 1 shows that the neutrino mass hierarchy and the relative sign assignment of the mass eigenvalues play crucial roles for the stability of the MNS matrix against quantum corrections.

5 Three generation neutrinos

Now let us discuss the stability of the MNS matrix against quantum corrections in three-generation case, according to the classification of the mass hierarchies in (1.4).

5.1 Type A ($m_1 \sim m_2 \ll m_3$)

In the Type A scenario, the mass spectrum is given by

$$\begin{aligned} &m_1 = 0\,, \quad m_2 = \sqrt{\Delta m^2_{\rm solar}}\,, \\ &m_3 = \sqrt{\Delta m^2_{\rm solar} + \Delta m^2_{\rm ATM}}\,. \end{aligned} \tag{5.1}$$

Neutrino masses of this type have large hierarchies. In this type, there are the following relative sign assignments for mass eigenvalues:

$$\text{case (a1):} \quad m_\nu^{\rm a1} = diag.(0, m_2, m_3)\,, \tag{5.2a}$$

$$\text{case (a2):} \quad m_\nu^{\rm a2} = diag.(0, -m_2, m_3)\,. \tag{5.2b}$$

The neutrino mass matrices at the weak scale for (a1) and (a2) are given in Table 2, where we write the leading order of each element, and the small parameter, ξ_a, is defined as

$$\xi_{\rm a} = \frac{m_2}{m_3} \simeq \sqrt{\frac{\Delta m^2_{\rm solar}}{\Delta m^2_{\rm ATM}}}\,. \tag{5.3}$$

The relation between the neutrino mass matrices at m_Z and M_R is given by

$$\begin{aligned} M_\nu(M_R) &= \begin{pmatrix} 1-\epsilon_e & 0 & 0 \\ 0 & 1-\epsilon_\mu & 0 \\ 0 & 0 & 1 \end{pmatrix} M_\nu(m_Z) \\ &\quad \times \begin{pmatrix} 1-\epsilon_e & 0 & 0 \\ 0 & 1-\epsilon_\mu & 0 \\ 0 & 0 & 1 \end{pmatrix}. \end{aligned} \tag{5.4}$$

The mixing angles of the MNS matrix at M_R can be obtained from (5.4). We denote the mixing angles at the M_R scale as $\hat{\theta}_{ij}$. Table 3 gives the $\tan\beta$ dependences of the mixing angles $\hat{\theta}_{ij}$ in the region $2 \le \tan\beta \le 60$. Here the initial conditions of the mixing angles θ_{ij} at the m_Z scale are given by (2.16) and (2.17) as the inputs. Table 3 shows that mixing angles are stable against quantum corrections in this scenario. For $U_{e3} \simeq 0$, the MNS matrix can be regarded as being two sets of two-generation mixings, one between the first and the second generations and the other between the second and the third generations. Since large mass hierarchies exist in the first and second generations and also in the second and third generations as $m_1 \ll m_2$ and $m_2 \ll m_3$, $\sin^2 2\hat{\theta}_{12}$ and $\sin^2 2\hat{\theta}_{23}$ are also stable against quantum corrections on the analogy of Type $\mathrm{A}^{(2)}$. Our numerical analyses show that all mixing angles are insensitive to quantum corrections even at $\tan\beta \simeq 60$. The MNS matrix is stable against quantum corrections in (a1) and (a2).

5.2 Type B ($m_1 \sim m_2 \gg m_3$)

At first we consider the case that m_1 is smaller than m_2. Then, the mass spectrum of this type is given by

$$\begin{aligned} &m_1 = \sqrt{\Delta m^2_{\rm ATM}}\,, \quad m_2 = \sqrt{\Delta m^2_{\rm ATM} + \Delta m^2_{\rm solar}}\,, \\ &m_3 = \sqrt{\Delta m^2_{\rm solar}}\,, \end{aligned} \tag{5.5}$$

Table 1. Stabilities of the two-generation case

hierarchy	$\kappa(m_Z)$	$\tan 2\hat{\theta}_{23}$(mixing angle at the M_R)	Stability
Type A$^{(2)}$ ($\kappa_3 \gg \kappa_2$)	$\kappa_3 \cos^2\theta_{23} \begin{pmatrix} \tan^2\theta_{23} & \tan\theta_{23} \\ \tan\theta_{23} & 1 \end{pmatrix}$	$\tan 2\theta_{23}\,(1-\epsilon\sec 2\theta_{23}) + O(\epsilon^2)$	stable
Type B1$^{(2)}$ ($\kappa_3 \simeq \kappa_2$)	$\left(\kappa_3 - \delta_k \sin^2\theta_{23}\right) \times \begin{pmatrix} 1-\frac{\delta_k}{\kappa_3}\cos 2\theta_{23} & \frac{\delta_k}{2\kappa_3}\sin 2\theta_{23} \\ \frac{\delta_k}{2\kappa_3}\sin 2\theta_{23} & 1 \end{pmatrix}$	$\simeq \frac{\delta_k \sin 2\theta_{23}}{\delta_k \cos 2\theta_{23} + 2\epsilon\kappa_3}$	unstable ($\epsilon > \frac{\delta_k}{\kappa_3}$)
Type B2$^{(2)}$ ($\kappa_3 \simeq -\kappa_2$)	$\kappa_3 \cos 2\theta_{23} \begin{pmatrix} -1 & \tan 2\theta_{23} \\ \tan 2\theta_{23} & 1 \end{pmatrix}$	$\tan 2\theta_{23} + O(\epsilon^2)$	stable

Table 2. Neutrino mass matrices at the weak scale for (a1) and (a2)

	neutrino mass matrix in the leading order	Stability
case(a1) $diag.(0, m_2, m_3)$	$\frac{m_3}{2}\begin{pmatrix} 2\xi_a \sin^2\theta & \xi_a \sin 2\theta/\sqrt{2} & -\xi_a \sin 2\theta/\sqrt{2} \\ \xi_a \sin 2\theta/\sqrt{2} & 1 & 1 \\ -\xi_a \sin 2\theta/\sqrt{2} & 1 & 1 \end{pmatrix}$	stable
case(a2) $diag.(0, -m_2, m_3)$	$\frac{m_3}{2}\begin{pmatrix} -2\xi_a \sin^2\theta & -\xi_a \sin 2\theta/\sqrt{2} & \xi_a \sin 2\theta/\sqrt{2} \\ -\xi_a \sin 2\theta/\sqrt{2} & 1 & 1 \\ \xi_a \sin 2\theta/\sqrt{2} & 1 & 1 \end{pmatrix}$	stable

Table 3. $\tan\beta$ dependences of the mixing angles at M_R in (a1) and (a2) ($2 \le \tan\beta \le 60$). The magnitudes of each mixing angles at the m_Z are (2.16) and (2.17)

		MSW-S	MSW-L	VO
(a1)	$\sin^2 2\hat{\theta}_{12}$	$0.007 \sim 0.006$	$1 \sim 0.996$	$1 \sim 0.996$
	$\sin^2 2\hat{\theta}_{23}$	$1 \sim 0.98$	$1 \sim 0.98$	$1 \sim 0.98$
	$\sin^2 2\hat{\theta}_{13}$	$0.0 \sim 2.7 \times 10^{-7}$	$0.0 \sim 8.8 \times 10^{-5}$	$0.0 \sim 3.7 \times 10^{-10}$
(a2)	$\sin^2 2\hat{\theta}_{12}$	$0.007 \sim 0.006$	$1 \sim 0.996$	$1 \sim 0.996$
	$\sin^2 2\hat{\theta}_{23}$	$1 \sim 0.98$	$1 \sim 0.98$	$1 \sim 0.98$
	$\sin^2 2\hat{\theta}_{13}$	$0.0 \sim 2.2 \times 10^{-7}$	$0.0 \sim 6.8 \times 10^{-5}$	$0.0 \sim 3.7 \times 10^{-10}$

Table 4. Neutrino mass matrices at m_Z for (b1) and (b2)

	neutrino mass matrix in the leading order	Stability
case(b1) $diag.(m_1, m_2, 0)$	$\frac{m_1}{2}\begin{pmatrix} 2 & \xi_b \sin 2\theta/\sqrt{2} & -\xi_b \sin 2\theta/\sqrt{2} \\ \xi_b \sin 2\theta/\sqrt{2} & 1 & -1 \\ -\xi_b \sin 2\theta/\sqrt{2} & -1 & 1 \end{pmatrix}$	unstable (θ_{12})
case(b2) $diag.(m_1, -m_2, 0)$	$-\frac{m_1 \cos 2\theta}{2}\begin{pmatrix} -2 & \sqrt{2}\tan 2\theta & -\sqrt{2}\tan 2\theta \\ \sqrt{2}\tan 2\theta & 1 & -1 \\ -\sqrt{2}\tan 2\theta & -1 & 1 \end{pmatrix}$	stable

Table 5. $\tan\beta$ dependences of the mixing angles at M_R in the case (b1) and (b2) ($2 \leq \tan\beta \leq 60$)

		MSW-S	MSW-L	VO
	$\sin^2 2\hat{\theta}_{12}$		see Figure 2	
(b1)	$\sin^2 2\hat{\theta}_{23}$	$1 \sim 0.98$	$1 \sim 0.98$	$1 \sim 0.98$
	$\sin^2 2\hat{\theta}_{13}$	0.0	0.0	0.0
	$\sin^2 2\hat{\theta}_{12}$	0.007	1	1
(b2)	$\sin^2 2\hat{\theta}_{23}$	$1 \sim 0.98$	$1 \sim 0.98$	$1 \sim 0.98$
	$\sin^2 2\hat{\theta}_{13}$	0.0	0.0	0.0

There are the following two relative sign assignments for the mass eigenvalues.

$$\text{case (b1):} \quad m_\nu^{b1} = diag.(m_1, m_2, 0)\,, \tag{5.6a}$$
$$\text{case (b2):} \quad m_\nu^{b2} = diag.(m_1, -m_2, 0)\,. \tag{5.6b}$$

The neutrino mass matrices in the leading order at m_Z for (b1) and (b2) are listed in Table 4, where the small parameter ξ_b is defined as

$$\xi_b = \frac{m_2 - m_1}{m_1} = \frac{1}{2}\ \frac{\Delta m^2_{\rm solar}}{\Delta m^2_{\rm ATM}}\,. \tag{5.7}$$

We analyze the stability of the MNS matrix for (b1) and (b2) against quantum corrections by using $M_\nu(M_R)$ obtained from (5.4). The results of our numerical analyses are listed in Table 5. Let us examine the details of the case (b1) first, and then (b2).

case(b1): Eigenvalues of $M_\nu(M_R)$, $\overline{m}_2 > \overline{m}_1 \gg \overline{m}_3$, are given by

$$\begin{aligned} &\overline{m}_1 = m_1\,(1+\xi_b)\ , \quad \overline{m}_2 = m_1\,(1-3\epsilon)\ , \\ &\overline{m}_3 = 0\,, \quad (|\xi_b| > 3|\epsilon|)\,, \\ &\overline{m}_1 = m_1\,(1-3\epsilon)\ , \quad \overline{m}_2 = m_1\,(1+\xi_b)\ , \\ &\overline{m}_3 = 0\,, \quad (|\xi_b| < 3|\epsilon|)\,, \end{aligned} \tag{5.8}$$

up to the order of ϵ and ξ_b for any value of θ.

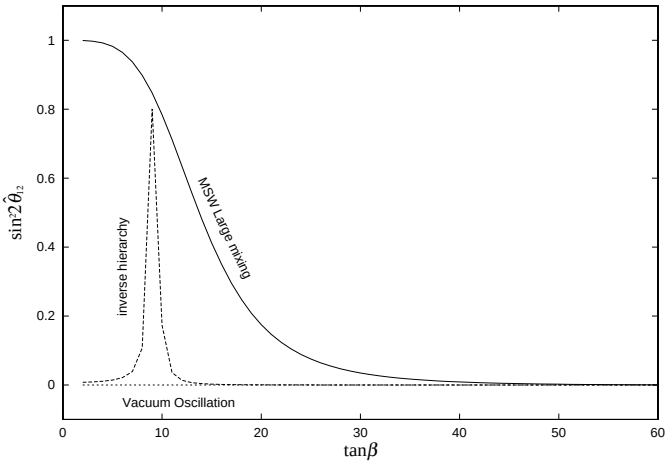

Fig. 2. $\tan\beta$ dependences of $\sin^2 2\hat{\theta}_{12}$ at $M_R = 10^{13}$GeV according to the solar neutrino solutions in (b1)

Numerical analyses of Table 5 suggest that $\sin^2 2\hat{\theta}_{13}$ and $\sin^2 2\hat{\theta}_{23}$ are stable against quantum corrections. This is because there are large hierarchies of $m_1 \ll m_3$ and $m_2 \ll m_3$ on the analogy of Type $A^{(2)}$. How about $\sin^2 2\hat{\theta}_{12}$? Figure 2 shows that $\tan\beta$ dependence of the $\sin^2 2\hat{\theta}_{12}$ corresponding to the MSW-L solution and the VO solution. As in the previous section, we use mixing angles at the m_Z scale in (2.16) and (2.17) as inputs parameters. For the MSW-S solution, the mixing angle $\hat{\theta}_{12}$ is stable against quantum corrections.

In the MSW-L solution, the magnitude of $\sin^2 2\hat{\theta}_{12}$ at the M_R scale is damped strongly from its initial values, $\sin^2 2\theta_{12} \sim 1$ at m_Z scale, if $\tan\beta \geq 20$. On the other hand, $\sin^2 2\hat{\theta}_{12} \simeq 0$ at M_R is obtained even in the small $\tan\beta$ region in case of the VO solution. The above two cases can be easily understood as follows. From (5.4), $\tan 2\hat{\theta}_{12}$ is estimated to be

$$\tan 2\hat{\theta}_{12} \simeq \tan 2\theta_{12}\ \left(1 + \frac{1}{\cos 2\theta_{12}}\frac{\epsilon}{|\xi_b|}\right)^{-1}\,, \tag{5.9}$$

where we define $\epsilon \equiv \epsilon_e \simeq \epsilon_\mu$. When θ_{12} is $\pi/4$, (5.9) becomes

$$\tan 2\hat{\theta}_{12} \simeq \frac{\xi_b}{2\epsilon} \sim \begin{cases} \dfrac{10^{-3}}{\epsilon}\ (\text{MSW-L})\,, \\ \dfrac{10^{-9}}{\epsilon}\ (\text{VO})\,, \end{cases} \tag{5.10}$$

from (5.7). Dotted-lines of (c) in Figures 1 shows that ϵ is much larger than 10^{-3} in the region of $\tan\beta > 20$. Then, from (5.10), $\sin^2 2\hat{\theta}_{12}$ is sufficiently small when $\tan\beta$ is larger than 20 in the MSW-L solution. On the other hand, (5.10) suggests $\sin^2 2\hat{\theta}_{12} \simeq 0$ even in the small $\tan\beta$ region in the VO solution.

Finally, let us see how the stability of the MNS matrix is changed if we take the mass spectrum as

$$m_1 = \sqrt{\Delta m^2_{\rm ATM} + \Delta m^2_{\rm solar}}\,, \quad m_2 = \sqrt{\Delta m^2_{\rm ATM}}\,, \quad m_3 = 0\,. \tag{5.11}$$

instead of (5.5). The behaviors of the mixing angles against quantum corrections for the MSW-L and the VO solutions are the same as those of (5.5).

For the MSW-S solution is not realistic one. It is because the dominant component of the heaviest state ν_1, (5.11) becomes ν_e in the MSW-S solution. Therefore the neutrino oscillation through matter effects is not realized in this mass spectrum. However, we discuss this mass spectrum with small mixing angle θ_{12}, which we call inverse hierarchy case, because interesting result is obtained. In this mass spectrum, (5.9) becomes

$$\tan 2\hat{\theta}_{12} \simeq \tan 2\theta_{12}\ \left(1 - \frac{1}{\cos 2\theta_{12}}\frac{\epsilon}{|\xi_b|}\right)^{-1}, \tag{5.12}$$

and (5.7) is replaced by

$$\xi_b = \frac{m_2 - m_1}{m_1} = -\frac{1}{2}\frac{\Delta m^2_{\rm solar}}{\Delta m^2_{\rm ATM}}\,. \tag{5.13}$$

In the MSW-S solution, $\sin^2 2\hat{\theta}_{12}$ has a peak around $\tan\beta \sim 10$. This peak depends on the M_R scale because the peak appears from cancellation among κ's elements. When $\theta_{12} \ll 1$, (5.12) becomes

$$\tan 2\hat{\theta}_{12} \simeq 2\theta_{12}\ \left(1 - \frac{\epsilon}{|\xi_b|}\right)^{-1}. \tag{5.14}$$

This means that $\tan 2\hat{\theta}_{12}$ diverges ($\sin^2 2\hat{\theta}_{12} \sim 1$) at $\epsilon \simeq |\xi_b|$. Equation (5.13) suggests that $|\xi_b|$ is about 10^{-3}. Figures 1 shows $\epsilon \simeq 10^{-3}$ around $\tan\beta \sim 10$ for $M_R = 10^{13}$GeV. Thus, $\sin^2 2\hat{\theta}_{12}$ becomes one at around $\tan\beta \sim 10$ almost independently of the value of θ_{12}. This is the reason why the peak in Fig. 2 appears in the inverse hierarchy case.

case(b2): Eigenvalues of $M_\nu(M_R)$ are given by

$$\overline{m}_1 = m_1\left(\sqrt{1+\xi_b-3\epsilon} + \frac{1}{2}\left(\xi_b + \epsilon\cos 2\theta\right)\right), \quad \overline{m}_2 = -m_1\left(\sqrt{1+\xi_b-3\epsilon} - \frac{1}{2}\left(\xi_b + \epsilon\cos 2\theta\right)\right), \quad \overline{m}_3 = 0\,, \tag{5.15}$$

up to the order of ϵ and ξ_b. Numerical analyses of Table 5 show that the MNS matrix is stable against quantum corrections. This can be easily understood as follows: $\sin^2 2\hat{\theta}_{13}$ and $\sin^2 2\hat{\theta}_{23}$ are stable against quantum corrections, because there are large hierarchies between the first and third generations and also between the second and third generations on the analogy of Type $A^{(2)}$; also $\sin^2 2\hat{\theta}_{12}$ is stable against quantum corrections since the signs of m_1 and m_2 are different from each other on the analogy of Type $B2^{(2)}$. Thus, we can conclude that all the MNS matrix elements are stable against quantum corrections in case (b2).

The results of (b1) and (b2) are consistent with the results in [10].

5.3 Type C ($m_1 \sim m_2 \sim m_3$)

The mass spectrum is given by

$$m_1 = m_0\,, \quad m_2 = \sqrt{m_0^2 + \Delta m^2_{\rm solar}}\,, \quad m_3 = \sqrt{m_0^2 + \Delta m^2_{\rm solar} + \Delta m^2_{\rm ATM}}\,, \tag{5.16}$$

where m_0 is the degenerate mass scale. We take $m_0 =$ 1.0 eV or 0.2 eV in this article. There are the following four different relative sign assignments of neutrino mass eigenvalues:

$$\text{case (c1):}\quad m_\nu^{c1} = diag.(-m_1, m_2, m_3)\,, \tag{5.17a}$$
$$\text{case (c2):}\quad m_\nu^{c2} = diag.(m_1, -m_2, m_3)\,, \tag{5.17b}$$
$$\text{case (c3):}\quad m_\nu^{c3} = diag.(-m_1, -m_2, m_3)\,, \tag{5.17c}$$
$$\text{case (c4):}\quad m_\nu^{c4} = diag.(m_1, m_2, m_3)\,. \tag{5.17d}$$

We define the small parameters

$$\delta_c \equiv \frac{m_3 - m_2}{m_0} \simeq \frac{1}{2}\frac{\Delta m^2_{\rm ATM}}{m_0^2}, \quad \xi_c \equiv \frac{m_2 - m_1}{m_0} \simeq \frac{1}{2}\frac{\Delta m^2_{\rm solar}}{m_0^2}\,, \tag{5.18}$$

where ξ_c is always smaller than δ_c. The neutrino mass matrices for all types are listed in Table 6 up to the leading order for each element.

In the case of $m_0 = 1.0$ eV, all three solar neutrino solutions of cases (c3) and (c4) and the MSW-S solution of the cases (c1) and (c2) have been excluded by the neutrino-less double-β decay experiments [23], whose upper limit is given by $\langle m_{\nu_e}\rangle < 0.2$ eV [24], where

$$\langle m_{\nu_e}\rangle = \left|\sum_{i=1}^{3} m_i\,(V_{\rm MNS})^2_{ei}\right|$$

Table 6. Neutrino mass matrices at m_Z for (c1) $\sim$ (c4)

	neutrino mass matrix up to the leading order	Stability
case(c1) $diag.(-m_1, m_2, m_3)$	$\frac{m_0}{2}\begin{pmatrix} -2\cos 2\theta & \sqrt{2}\sin 2\theta & -\sqrt{2}\sin 2\theta \\ \sqrt{2}\sin 2\theta & 1+\cos 2\theta & 1-\cos 2\theta \\ -\sqrt{2}\sin 2\theta & 1-\cos 2\theta & 1+\cos 2\theta \end{pmatrix}$	rearrangement between V_2 and V_3
case(c2) $diag.(m_1, -m_2, m_3)$	$\frac{m_0}{2}\begin{pmatrix} 2\cos 2\theta & -\sqrt{2}\sin 2\theta & \sqrt{2}\sin 2\theta \\ -\sqrt{2}\sin 2\theta & 1-\cos 2\theta & 1+\cos 2\theta \\ \sqrt{2}\sin 2\theta & 1+\cos 2\theta & 1-\cos 2\theta \end{pmatrix}$	rearrangement between V_1 and V_3
case(c3) $diag.(-m_1, -m_2, m_3)$	$m_0\begin{pmatrix} -1 & -\sqrt{2}\xi_c\sin 2\theta & \sqrt{2}\xi_c\sin 2\theta \\ -\sqrt{2}\xi_c\sin 2\theta & \delta_c/2 & 1 \\ \sqrt{2}\xi_c\sin 2\theta & 1 & \delta_c/2 \end{pmatrix}$	rearrangement between V_1 and V_2
case(c4) $diag.(m_1, m_2, m_3)$	$m_0\begin{pmatrix} 1 & \sqrt{2}\xi_c\sin 2\theta & -\sqrt{2}\xi_c\sin 2\theta \\ \sqrt{2}\xi_c\sin 2\theta & 1 & \delta_c/2 \\ -\sqrt{2}\xi_c\sin 2\theta & \delta_c/2 & 1 \end{pmatrix}$	unstable go to the unit matrix

$$= \begin{cases} m_0\left(\cos 2\theta - \xi_c \sin^2\theta\right), \\ \quad \text{(for case (c1) and (c2))}, \\ m_0\left(1 + \xi_c \sin^2\theta\right), \\ \quad \text{(for case (c3) and (c4))}, \end{cases} \tag{5.19}$$

from (2.16) and (5.18). Thus, we analyze the stability of the MNS matrix for (c1) and (c2) with $m_0 = 1.0$ eV, and for all cases with $m_0 = 0.2$ eV.

5.3.1 $m_0 = 1.0$ eV

Figures 3 show the $\tan\beta$ dependence of $\sin^2 2\hat{\theta}_{ij}$ in (c1) and (c2) for $m_0 = 1.0$ eV. They show that all $\sin^2 2\hat{\theta}_{ij}$'s gradually approach fixed values as $\tan\beta$ becomes large. We can estimate the value of $\tan\beta$ where the mixing angles become close to the fixed values.

The dotted-line of (b) in Figure 1 show the value of

$$\delta_c = \frac{\Delta m^2_{\rm ATM}}{2m_0^2} = 1.9 \times 10^{-3}, \qquad (m_0 = 1.0 \text{ eV}). \tag{5.20}$$

We can see that $\delta_c \ll \epsilon$ for $\tan\beta \geq 20$ in Fig. 1. As $\tan\beta$ increases, the quantum effects become larger than the effects of the mass-squared differences of neutrinos. All $\sin^2 2\hat{\theta}_{ij}$s approach their fixed values at around $\tan\beta \sim 20$ as shown in Figures 3.

By taking the limit of $\delta_c \ll \epsilon$ we can obtain the fixed values of $\sin^2 2\hat{\theta}_{ij}$ according to the solar neutrino solutions in (c1) and (c2) as follows:

case (c1): The eigenvectors $V_{1,2,3}$ at the m_Z scale are given by

$$V_1 = \begin{pmatrix} \cos\theta \\ \frac{-1}{\sqrt{2}}\sin\theta \\ \frac{1}{\sqrt{2}}\sin\theta \end{pmatrix}, \quad V_2 = \begin{pmatrix} \sin\theta \\ \frac{1}{\sqrt{2}}\cos\theta \\ \frac{-1}{\sqrt{2}}\cos\theta \end{pmatrix}, \quad V_3 = \begin{pmatrix} 0 \\ \frac{1}{\sqrt{2}} \\ \frac{1}{\sqrt{2}} \end{pmatrix}. \tag{5.21}$$

V_i is the eigenvector of the i-th eigenvalue of the neutrino mass matrix, which corresponds to each column of the MNS matrix in (2.16). At the M_R scale, eigenvalues of (5.4) are given by

$$\begin{aligned} m_1(M_R) &= -m_0(1 - \epsilon(1+\cos^2\theta)), \\ m_2(M_R) &= m_0(1-2\epsilon), \\ m_3(M_R) &= m_0(1-\epsilon\sin^2\theta), \end{aligned} \tag{5.22}$$

up to the order ϵ under the condition $\delta_c \ll \epsilon$. Their eigenvectors are

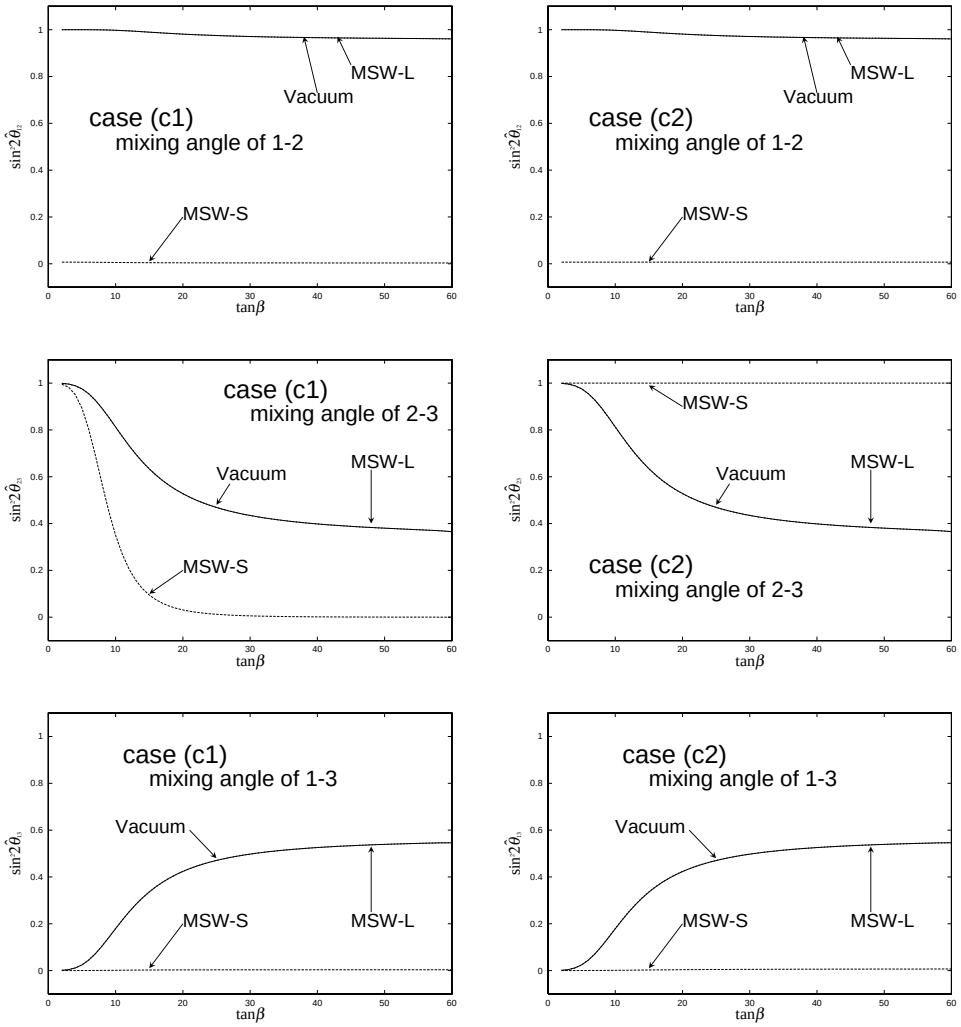

Fig. 3a–f. $\tan\beta$ dependences of $\sin^2 2\hat{\theta}_{ij}$ at $M_R = 10^{13}$GeV in (c1) and (c2) for $m_0 = 1.0$ eV

$$V_1' = \begin{pmatrix} \cos\theta \\ -\dfrac{\sin\theta}{\sqrt{2}} \\ \dfrac{\sin\theta}{\sqrt{2}} \end{pmatrix}, \quad V_2' = \begin{pmatrix} \dfrac{\sin\theta}{\sqrt{1+\cos^2\theta}} \\ \dfrac{\sqrt{2}\cos\theta}{\sqrt{1+\cos^2\theta}} \\ 0 \end{pmatrix},$$

$$V_3' = \begin{pmatrix} -\dfrac{1}{2}\dfrac{\sin 2\theta}{\sqrt{1+\cos^2\theta}} \\ \dfrac{1}{\sqrt{2}}\dfrac{\sin^2\theta}{\sqrt{1+\cos^2\theta}} \\ \dfrac{1}{\sqrt{2}}\sqrt{1+\cos^2\theta} \end{pmatrix}. \qquad (5.23)$$

By comparing (5.21) with (5.23), the relation between V_i and V_i' is given by

$$\begin{pmatrix} V_1' \\ V_2' \\ V_3' \end{pmatrix} = \begin{pmatrix} 1 & 0 & 0 \\ 0 & \dfrac{1}{\sqrt{1+\cos^2\theta}} & \dfrac{\cos\theta}{\sqrt{1+\cos^2\theta}} \\ 0 & \dfrac{-\cos\theta}{\sqrt{1+\cos^2\theta}} & \dfrac{1}{\sqrt{1+\cos^2\theta}} \end{pmatrix} \times \begin{pmatrix} V_1 \\ V_2 \\ V_3 \end{pmatrix}. \qquad (5.24)$$

When we take $\theta = \pi/4$ ($\theta = 0$) in (5.24), we can obtain the relation between V_i and V_i' for the MSW-L and the VO solutions (the MSW-S solution).

For the MSW-L and the VO solutions, the MNS matrix at the M_R scale is given by

$$\hat{U}_{\rm MNS} = \begin{pmatrix} 1/\sqrt{2} & 1/\sqrt{3} & -1/\sqrt{6} \\ -1/2 & 2/\sqrt{3} & 1/2\sqrt{3} \\ 1/2 & 0 & \sqrt{3}/2 \end{pmatrix} \tag{5.25}$$

in the limit of $\delta_c \ll \epsilon$. The relation between V_i and V_i' is given by

$$\begin{aligned} &V_1' = V_1\,, \qquad V_2' = \sqrt{\frac{2}{3}}\,V_2 + \sqrt{\frac{1}{3}}\,V_3\,, \\ &V_3' = -\sqrt{\frac{1}{3}}\,V_2 + \sqrt{\frac{2}{3}}\,V_3\,. \end{aligned} \tag{5.26}$$

This is consistent with the results in [9].

For the MSW-S solution[4], the MNS matrix at the M_R is given by

$$\hat{U}_{\rm MNS} = \begin{pmatrix} 1\,0\,0 \\ 0\,1\,0 \\ 0\,0\,1 \end{pmatrix}\,, \tag{5.27}$$

which means

$$\begin{aligned} &V_1' = V_1\,, \qquad V_2' = \frac{1}{\sqrt{2}}\,V_2 + \frac{1}{\sqrt{2}}\,V_3\,, \\ &V_3' = -\frac{1}{\sqrt{2}}\,V_2 + \frac{1}{\sqrt{2}}\,V_3\,. \end{aligned} \tag{5.28}$$

case (c2): By the same calculations as those of (c1), the eigenvalues of (5.4) are obtained as

$$\begin{aligned} &m_1(M_R) = m_0(1-2\epsilon)\,, \\ &m_2(M_R) = -m_0(1-\epsilon(1+\sin^2\theta))\,, \\ &m_3(M_R) = m_0(1-\epsilon\cos^2\theta)\,, \end{aligned} \tag{5.29}$$

up to $O(\epsilon)$ in $\delta_c \ll \epsilon$. Their eigenvectors are given by

$$V_1' = \begin{pmatrix} \dfrac{\cos\theta}{\sqrt{1+\sin^2\theta}} \\ -\dfrac{\sqrt{2}\sin\theta}{\sqrt{1+\sin^2\theta}} \\ 0 \end{pmatrix}, \quad V_2' = \begin{pmatrix} \sin\theta \\ \dfrac{\cos\theta}{\sqrt{2}} \\ -\dfrac{\cos\theta}{\sqrt{2}} \end{pmatrix},$$

$$V_3' = \begin{pmatrix} \dfrac{1}{2}\dfrac{\sin 2\theta}{\sqrt{1+\sin^2\theta}} \\ \dfrac{1}{\sqrt{2}}\dfrac{\cos^2\theta}{\sqrt{1+\sin^2\theta}} \\ \dfrac{1}{\sqrt{2}}\sqrt{1+\sin^2\theta} \end{pmatrix}. \tag{5.30}$$

[4] Although the MSW-S solution in (c1) and (c2) with $m_0 = 1.0$ eV is already excluded by the neutrino-less double-β decay experiments of (5.19), we discuss it here to check if our analytic calculations are consistent with our numerical results.

By comparing (5.21) with (5.30), the relation between V_i and V_i' is given by

$$\begin{pmatrix} V_1' \\ V_2' \\ V_3' \end{pmatrix} = \begin{pmatrix} \dfrac{1}{\sqrt{1+\sin^2\theta}} & 0 & \dfrac{-\sin\theta}{\sqrt{1+\sin^2\theta}} \\ 0 & 1 & 0 \\ \dfrac{\sin\theta}{\sqrt{1+\sin^2\theta}} & 0 & \dfrac{1}{\sqrt{1+\sin^2\theta}} \end{pmatrix} \times \begin{pmatrix} V_1 \\ V_2 \\ V_3 \end{pmatrix}. \tag{5.31}$$

For the MSW-L and the VO solutions, the MNS matrix at the M_R scale is given by

$$\hat{U}_{\rm MNS} = \begin{pmatrix} 1/\sqrt{3} & 1/\sqrt{2} & 1/\sqrt{6} \\ -\sqrt{2/3} & 1/2 & 1/2\sqrt{3} \\ 0 & -1/2 & \sqrt{3}/2 \end{pmatrix} \tag{5.32}$$

in $\delta_c \ll \epsilon$. This means

$$\begin{aligned} &V_2' = V_2\,, \qquad V_1' = \sqrt{\frac{2}{3}}\,V_1 - \sqrt{\frac{1}{3}}\,V_3\,, \\ &V_3' = \sqrt{\frac{1}{3}}\,V_1 + \sqrt{\frac{2}{3}}\,V_3\,. \end{aligned} \tag{5.33}$$

This is consistent with the results in [8].

For the MSW-S solution[4], the MNS matrix at the M_R scale is obtained as

$$\hat{U}_{\rm MNS} = \begin{pmatrix} 1 & 0 & 0 \\ 0 & 1/\sqrt{2} & 1/\sqrt{2} \\ 0 & -1\sqrt{2} & 1/\sqrt{2} \end{pmatrix}\,, \tag{5.34}$$

which suggests

$$V_1' = V_1\,, \qquad V_2' = V_2\,, \qquad V_3' = V_3\,. \tag{5.35}$$

For the MSW-L and the VO solutions in (c1) and (c2), (5.25) and (5.32) suggest the fixed values of the $\sin^2 2\hat{\theta}_{ij}$s are

$$\sin^2 2\hat{\theta}_{12} = 0.96\,, \quad \sin^2 2\hat{\theta}_{23} = 0.36\,, \quad \sin^2 2\hat{\theta}_{13} = \frac{5}{9}\,, \tag{5.36}$$

in the limit of $\epsilon \gg \delta_c$. We cannot see the differences between the MSW-L and the VO solutions in Figures 3. It is because the value of $\tan\beta$ where all $\sin^2 2\hat{\theta}_{ij}$s approach their fixed values are determined by ϵ and δ_c which is solely determined by $\Delta m^2_{\rm ATM}$. The rearrangements occur between V_2 and V_3 in (c1), and V_1 and V_3 in (c2), where the squared mass differences of their eigen-values

are mainly determined by $\Delta m^2_{\rm ATM}$. On the other hand, for the MSW-S solution (5.27) and (5.34) suggest that all of the mixing angles approach zero in the case of (c1), and $\sin^2 2\hat{\theta}_{12} = \sin^2 2\hat{\theta}_{13} = 0$, $\sin^2 2\hat{\theta}_{23} = 1$ in the case of (c2). These results from analytic calculations are completely consistent with those from numerical analyses, as shown in Fig. 3.

5.3.2 $m_0 = 0.2$ eV

Figures 4, 5, 6 and 7 show the $\tan\beta$ dependences of $\sin^2 2\hat{\theta}_{ij}$s with $m_0 = 0.2$ eV in (c1), (c2), (c3) and (c4), respectively.

cases (c1) and (c2): Figures 4 and 5 show that all $\sin^2 2\hat{\theta}_{ij}$s approach the same fixed values as those with $m_0 = 1.0$ eV in the large $\tan\beta$ region. However, the value of $\tan\beta$ where $\sin^2 2\hat{\theta}_{ij}$s becomes close to their fixed values with $m_0 = 0.2$ eV is larger than that with $m_0 = 1.0$ eV. The value of δ_c with $m_0 = 0.2$ eV is given by

$$\delta_c = \frac{\Delta m^2_{\rm ATM}}{2m_0^2} = 4.6 \times 10^{-2}\,, \qquad (m_0 = 0.2 \text{ eV})\,, \quad (5.37)$$

which is shown by the dotted-line (a) in Fig. 1. In the region of $2 \leq \tan\beta < 50$, ϵ is not larger than δ_c, and the first two generation neutrinos will not become degenerate with the third-generation neutrino. Thus, a rearrangement between the eigenvectors of $V_1(V_2)$ and V_3 is not completely realized, although the sign of $m_1(m_2)$ is the same as that of m_3.

case (c3): Figures 6 show that for all solar neutrino solutions $\sin^2 2\hat{\theta}_{12}$ and $\sin^2 2\hat{\theta}_{13}$ are almost zero in the region of $\tan\beta \geq 10$, and $\sin^2 2\hat{\theta}_{23} \simeq 1$ in all $\tan\beta$ region. Up to the $O(\epsilon)$ eigenvalues of (5.4) are given by

$$\begin{aligned} m_1(M_R) &= -m_0(1-2\epsilon)\,, \\ m_2(M_R) &= -m_0(1-\epsilon)\,, \\ m_3(M_R) &= m_0(1-\epsilon)\,, \end{aligned} \quad (5.38)$$

and their eigenvectors are given by

$$V_1' = \begin{pmatrix} 1 \\ 0 \\ 0 \end{pmatrix}, \quad V_2' = \begin{pmatrix} 0 \\ 1/\sqrt{2} \\ -1/\sqrt{2} \end{pmatrix}, \quad V_3' = \begin{pmatrix} 0 \\ 1/\sqrt{2} \\ 1/\sqrt{2} \end{pmatrix}. \quad (5.39)$$

These eigenvectors and eigenvalues do not depend on the mixing angle, θ. Equations (5.39) suggest

$$\sin^2 2\hat{\theta}_{12} = 0\,, \qquad \sin^2 2\hat{\theta}_{23} = 1\,, \qquad \sin^2 2\hat{\theta}_{13} = 0\,, \quad (5.40)$$

from (2.7) in the region of $\xi_c \ll \epsilon$. By comparing (5.21) with (5.39), we can obtain

$$\begin{pmatrix} V_1' \\ V_2' \\ V_3' \end{pmatrix} = \begin{pmatrix} \cos\theta & \sin\theta & 0 \\ -\sin\theta & \cos\theta & 0 \\ 0 & 0 & 1 \end{pmatrix} \begin{pmatrix} V_1 \\ V_2 \\ V_3 \end{pmatrix}. \quad (5.41)$$

The rearrangement between V_1 and V_2 is realized, because the sign of m_1 is the same as that of m_2.

Figures 6 show $\sin^2 2\theta_{13}$ and $\sin^2 2\theta_{23}$ are not changed against quantum corrections, and $\sin^2 2\hat{\theta}_{12}$ is close to zero in $\tan\beta \geq 10$ for the MSW-L solution, while $\sin^2 2\hat{\theta}_{12} \simeq 0$ in all $\tan\beta$ region for the VO solution. These situations can be explained by estimating the value of $\tan\beta$ where the mixing angles are close to the fixed values. For the MSW-L solution, the value of ξ_c is given by

$$\xi_c = \frac{\Delta m^2_{\rm MSW-L}}{2m_0^2} = 2.3 \times 10^{-4}\,, \quad (5.42)$$

which is shown as dotted-lines of (d) in Fig. 1. Since ξ_c is much smaller than ϵ in the region $10 \leq \tan\beta$, the first and the second generations are regarded as being degenerate at m_0, and a rearrangement between V_1 and V_2 is realized. On the other hand, the VO solution gives the value of ξ_c as

$$\xi_c = \frac{\Delta m^2_{\rm VO}}{2m_0^2} = 1.1 \times 10^{-9}\,, \quad (5.43)$$

which is much smaller than ϵ in all $\tan\beta$ regions. Therefor, a rearrangement between V_1 and V_2 is realized even in the small $\tan\beta$ region for the VO solution.

case (c4): Figures 7 show that all $\sin^2 2\hat{\theta}_{ij}$s approach zero in the large $\tan\beta$ region. This means that the MNS matrix becomes the unit matrix in the limit of $\epsilon \gg \delta_c$. In the case of (c4) we cannot obtain the rearrangement rule between V_i and V_i', because κ becomes proportional to the unit matrix, which can be diagonalized by any unitary matrices.

Let us first see the MSW-L solution. Figure 1 shows $\xi_c \ll \delta_c \sim \epsilon$ in the region $10 < \tan\beta < 50$, where the value of ξ_c (δ_c) is shown in (5.42) ((5.37)). In this region (5.4) becomes

$$M_\nu(M_R) \simeq m_0 \begin{pmatrix} 1-2\epsilon & 0 & 0 \\ 0 & (1-2\epsilon) & (1-\epsilon)\,\delta_c/2 \\ 0 & (1-\epsilon)\,\delta_c/2 & 1 \end{pmatrix}. \quad (5.44)$$

This means that $\sin^2 2\hat{\theta}_{12}$ approaches to zero if $10 < \tan\beta$. Equation (5.44) also suggests the mixing between the second and the third generations becomes

$$\tan 2\hat{\theta}_{23} \simeq \frac{\delta_c}{2\epsilon}\,. \quad (5.45)$$

If $\tan\beta > 50$, ϵ is larger than δ_c, and $\sin^2 2\hat{\theta}_{23}$ becomes small as we can see in Figures 7.

For the VO solution, since the value of ξ_c in (5.43) is much smaller than values of ϵ and δ_c, $M_\nu(M_R)$ also becomes (5.44) in all $\tan\beta$ region. Therefor, $\sin^2 2\hat{\theta}_{12}$ and $\sin^2 2\hat{\theta}_{13}$ are zero at any value of $\tan\beta$. The behavior of $\sin^2 2\hat{\theta}_{23}$ in the VO solution is the same as that in the MSW-L solution, since (5.44) is independent of ξ_c.

Since the mixing angle $\theta \simeq 0$ for the MSW-S solution, $M_\nu(M_R)$ also becomes (5.44). Thus, $\sin^2 2\hat{\theta}_{12}$ and

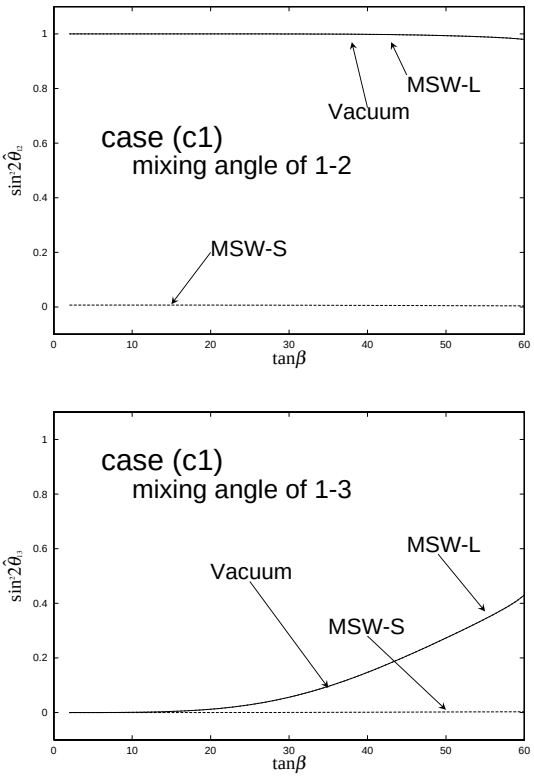

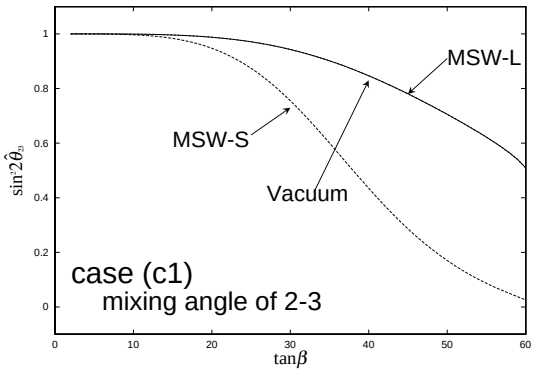

Fig. 4. $\tan\beta$ dependences of $\sin^2 2\hat{\theta}_{ij}$ in (c1) with $m_0 = 0.2$ eV

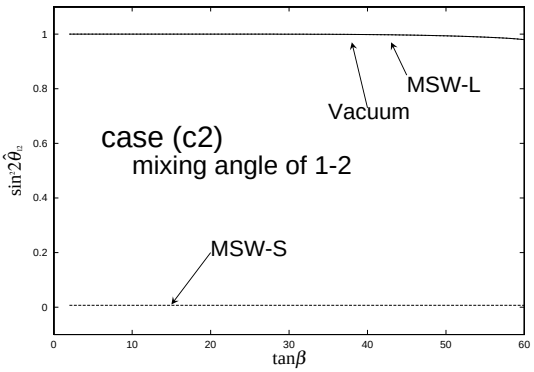

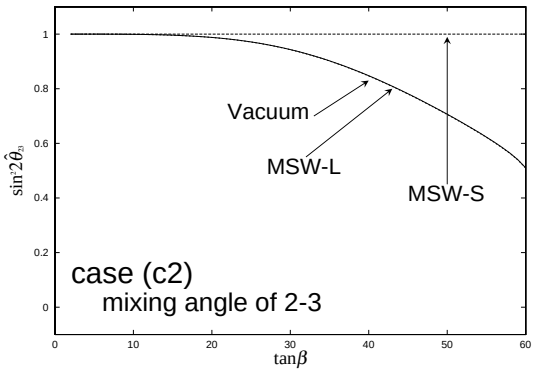

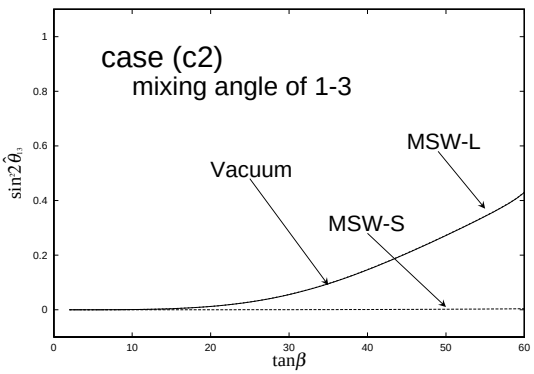

Fig. 5. $\tan\beta$ dependences of $\sin^2 2\hat{\theta}_{ij}$ in (c2) with $m_0 = 0.2$ eV

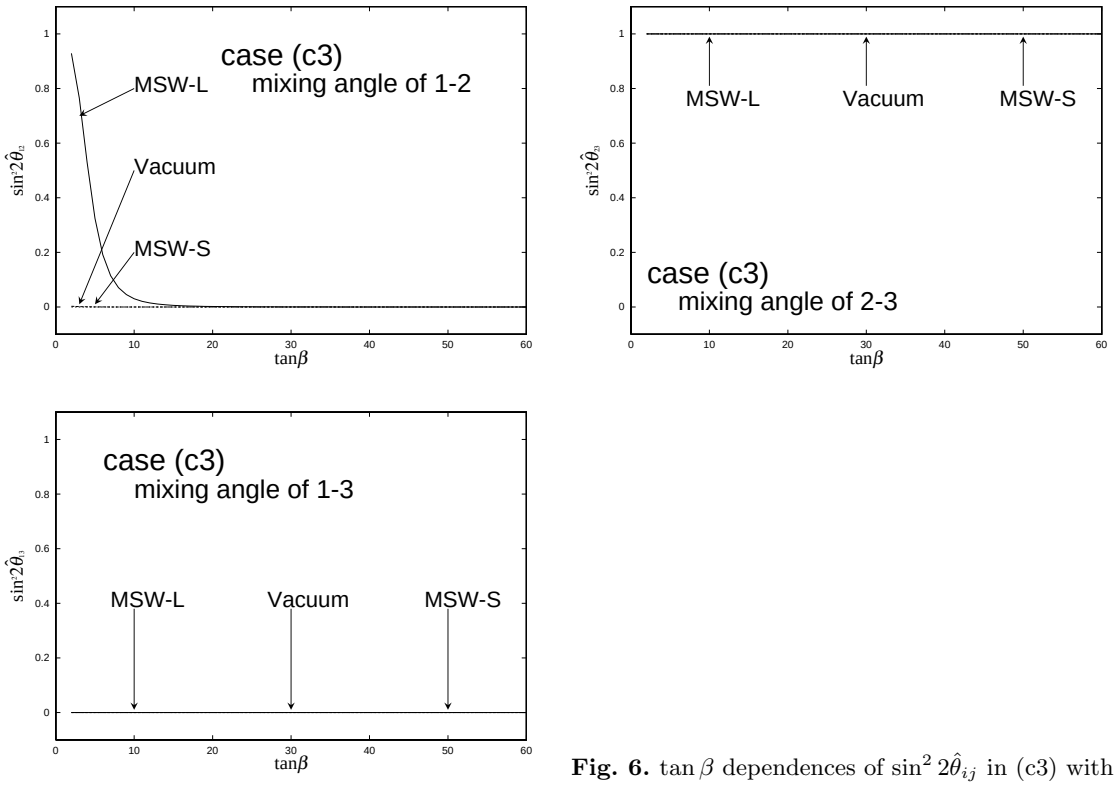

Fig. 6. $\tan\beta$ dependences of $\sin^2 2\hat{\theta}_{ij}$ in (c3) with $m_0 = 0.2$ eV

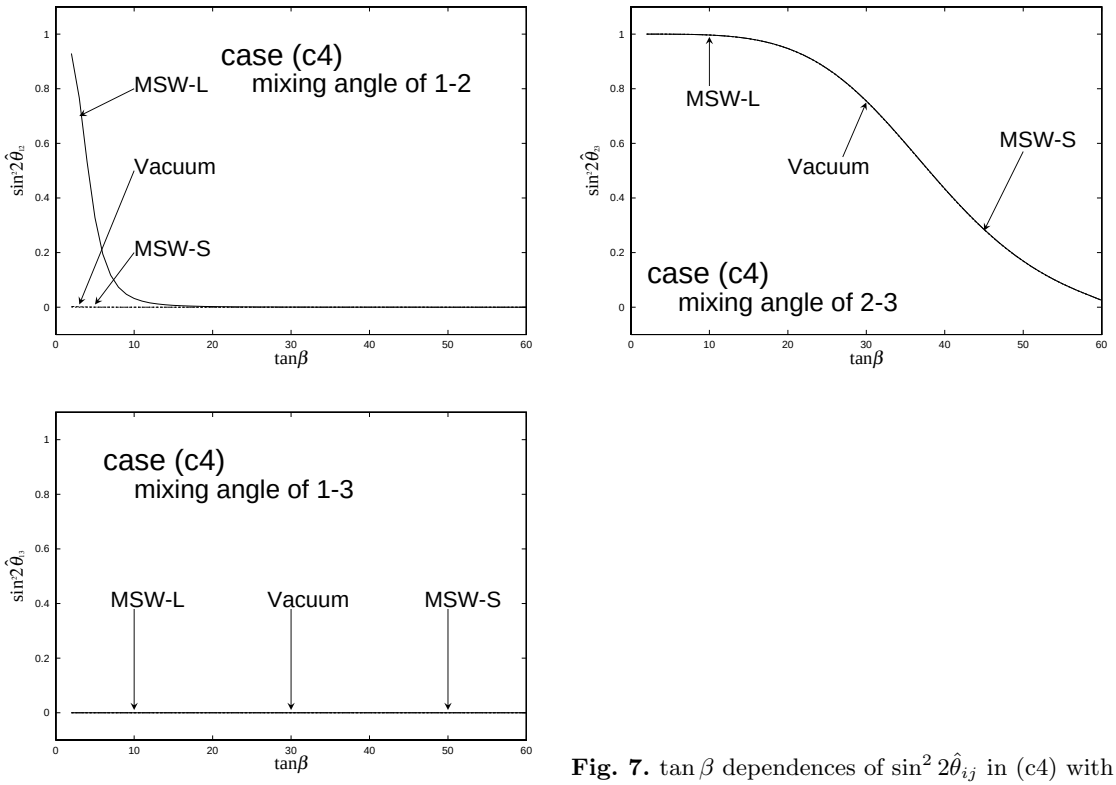

Fig. 7. $\tan\beta$ dependences of $\sin^2 2\hat{\theta}_{ij}$ in (c4) with $m_0 = 0.2$ eV

$\sin^2 2\hat{\theta}_{13}$ are zero in all $\tan\beta$ region, and $\tan\beta$ dependence of $\sin^2 2\hat{\theta}_{23}$ is the same as that in the MSW-L (VO) solution.

If we take the limit of $m_0 \to 0$, cases of type C become cases of Type A, where δ_c and ξ_c diverge infinities and are always larger than ϵ. It also suggests that all cases of Type A are stable against quantum corrections.

6 Conclusion

In this article, we study the stability of the Maki-Nakagawa-Sakata (MNS) lepton-flavor mixing matrix against quantum corrections in the minimal supersymmetric Standard Model (MSSM) with effective dimension-five operators which give the Majorana masses of neutrinos. We constrain the parameters of the MNS matrix at the weak scale based on experimental data, and obtain the MNS matrix at the high-energy scale (the right-handed neutrino decoupling scale M_R) by calculating the quantum corrections. Then, we analyze the stability of the MNS matrix between low and high energy scale according to the types of neutrino mass hierarchy.

In the two-generation neutrino case, the mixing angles for large mass hierarchy ($\kappa_3 \gg \kappa_2$), which we call Type $A^{(2)}$ and for degenerate neutrino masses with opposite sign of the eigenvalues ($\kappa_3 \simeq -\kappa_2$), which we call Type $B2^{(2)}$ are stable against quantum corrections. Here κ_2 and κ_3 are eigenvalues of the 2×2 neutrino mass matrix at the weak scale, where $|\kappa_i| = m_i$. The mixing angle for degenerate neutrino masses with same sign of the eigenvalues ($\kappa_3 \simeq \kappa_2$), which we call Type $B1^{(2)}$ is unstable around $\theta_{23} = \pi/4$ when the magnitude of the quantum correction, ϵ, is larger than $|(\kappa_3 - \kappa_2)/\kappa_3|$.

In the three-generation neutrinos, the stability of the MNS matrix strongly depends on the types of mass hierarchy and the relative sign assignments of mass eigenvalues. The results are summarized as follows:

1. Type A ($m_1 \sim m_2 \ll m_3$)
   The MNS matrix is stable against quantum corrections.
2. Type B ($m_1 \sim m_2 \gg m_3$)
   $\sin^2 2\theta_{13}$ and $\sin^2 2\theta_{23}$ are stable against quantum corrections because there are large hierarchies between the first and the third generations and also between the second and the third generations on the analogy of Type $A^{(2)}$,
   case (b1): $(\kappa_1, \kappa_2, \kappa_3) = (m_1, m_2, 0)$
   $\sin^2 2\theta_{12}$ is unstable against quantum corrections, when we assume that the solar neutrino deficit explain the MSW-L solution or the VO solution. This is understood on the analogy of Type $B1^{(2)}$. Thus, the MNS matrix is unstable against quantum corrections for both solutions. On the other hand, the MNS matrix is stable against quantum corrections for the MSW-S solution.
   case (b2): $(\kappa_1, \kappa_2, \kappa_3) = (m_1, -m_2, 0)$
   $\sin^2 2\hat{\theta}_{12}$ is also stable against quantum corrections analogous to the case of Type $B2^{(2)}$. The MNS matrix is stable against quantum corrections.
   The results of the case (b1) and (b2) are consistent with those of [10].
3. Type C ($m_1 \sim m_2 \sim m_3$)
   The MNS matrix approaches the definite unitary matrix according to the relative sign assignments of the neutrino mass eigenvalues, as the effects of quantum corrections become large enough to neglect the squared-mass differences of neutrinos. Independent parameters of the MNS matrix at the M_R scale approach the following fixed values in the large limit of quantum corrections:
   case (c1): $diag.(-m_1, m_2, m_3)$

$$U_{e2} = \frac{\sin\theta}{\sqrt{1+\cos^2\theta}}\,, \quad U_{e3} = -\frac{1}{2}\frac{\sin 2\theta}{\sqrt{1+\cos^2\theta}}\,,$$
$$U_{\mu 3} = \frac{1}{\sqrt{2}}\frac{\sin^2\theta}{\sqrt{1+\cos^2\theta}}\,. \tag{6.1}$$

   case (c2): $diag.(m_1, -m_2, m_3)$

$$U_{e2} = \sin\theta\,, \quad U_{e3} = \frac{1}{2}\frac{\sin 2\theta}{\sqrt{1+\sin^2\theta}}\,,$$
$$U_{\mu 3} = \frac{1}{\sqrt{2}}\frac{\cos^2\theta}{\sqrt{1+\sin^2\theta}}\,. \tag{6.2}$$

   case (c3): $diag.(-m_1, -m_2, m_3)$

$$U_{e2} = 0\,, \quad U_{e3} = 0\,, \quad U_{\mu 3} = \frac{1}{\sqrt{2}}\,. \tag{6.3}$$

   case (c4): $diag.(m_1, m_2, m_3)$

$$U_{e2} = 0\,, \quad U_{e3} = 0\,, \quad U_{\mu 3} = 0\,. \tag{6.4}$$

In the case (c1), our result is consistent with that of [9]. In the case (c2), the relation between eigenvectors at the m_Z scale and that at the M_R scale is the same as that of [8] in the large $\tan\beta$ region.

The results of this article are not only useful for model building, but also show the possibility to obtain large mixing angles from quantum corrections.

Acknowledgements. One of the author NO thanks G.-C. Cho and K. Hagiwara for useful discussion and comments. The work of NH is partially supported by DOE grant DOE/ER/01545-753. The work of NO is supported by the JSPS Research Fellowships for Young Scientists, No. 2996.

A Quantum corrections of κ when $\kappa_{33} = 0$

In this section, we show the relation between $\kappa(m_Z)$ and $\kappa(M_R)$ in the cases of $\kappa_{33} = 0$.

A.1 $\kappa_{33} = 0$, κ_{22} and $\kappa_{11} \neq 0$

At first, we discuss the case of $\kappa_{33} = 0$ in the diagonal base of $y^{\rm e}$. If some elements of κ are zero at m_Z, they are always zero at all energies. This means if κ_{33} is zero at m_Z, κ cannot be normalized by κ_{33} and c_{ij} of (3.3) cannot be defined. Thus, if $\kappa_{22} \neq 0$, we adopt κ_{22} for the normalization of κ as

$$\begin{aligned}\kappa &= \kappa_{22}\begin{pmatrix} r'_1 & c'_{12}\sqrt{r'_1} & c'_{13}r'_2\sqrt{r'_1} \\ c'_{12}\sqrt{r'_1} & 1 & r'_2 \\ c'_{13}r'_2\sqrt{r'_1} & r'_2 & 0 \end{pmatrix}, \\ &= \kappa_{22}\begin{pmatrix} \sqrt{r'_1} & 0 & 0 \\ 0 & 1 & 0 \\ 0 & 0 & r'_2 \end{pmatrix}\begin{pmatrix} 1 & c'_{12} & c'_{13} \\ c'_{12} & 1 & 1 \\ c'_{13} & 1 & 0 \end{pmatrix} \\ &\quad\times\begin{pmatrix} \sqrt{r'_1} & 0 & 0 \\ 0 & 1 & 0 \\ 0 & 0 & r'_2 \end{pmatrix}, \end{aligned} \tag{A.1}$$

where c'_{1j}s $(j = 2, 3)$ are defined as

$$\left(c'_{12}\right)^2 = \frac{\kappa_{12}^2}{\kappa_{11}\kappa_{22}}, \quad \text{and} \quad \left(c'_{13}\right)^2 = \frac{\kappa_{22}\kappa_{13}^2}{\kappa_{11}\kappa_{23}^2}, \tag{A.2}$$

which are energy-scale independent complex parameters. $r'_{1,2}$ in (A.1) are defined as

$$\begin{aligned} r'_1 &= \frac{\kappa_{11}}{\kappa_{22}}, \\ r'_2 &= \frac{\kappa_{23}}{\kappa_{22}}. \end{aligned} \tag{A.3}$$

By using the notation of (3.8), we can obtain the energy-scale dependences of $r'_{1,2}$ as

$$\begin{aligned} r'_1(M_R) &= r'_1(m_Z)\frac{I_e}{I_\mu}, \\ r'_2(M_R) &= r'_2(m_Z)\sqrt{\frac{I_\tau}{I_\mu}}. \end{aligned} \tag{A.4}$$

Then, $\kappa(M_R)$ is given by

$$\begin{aligned}\kappa(M_R) &= \frac{k_{22}(M_R)}{k_{22}(m_Z)}\frac{I_\tau}{I_\mu}\begin{pmatrix} \sqrt{I_e/I_\tau} & 0 & 0 \\ 0 & \sqrt{I_\mu/I_\tau}\,0 & \\ 0 & 0 & 1 \end{pmatrix}\kappa(m_Z) \\ &\quad\times\begin{pmatrix} \sqrt{I_e/I_\tau} & 0 & 0 \\ 0 & \sqrt{I_\mu/I_\tau}\,0 & \\ 0 & 0 & 1 \end{pmatrix}. \end{aligned} \tag{A.5}$$

A.2 $\kappa_{11} = \kappa_{22} = \kappa_{33} = 0$

When all diagonal elements are zero, all off-diagonal elements of κ can be taken to be real. This is because all phases are absorbed by the field redefinitions of

$$L_i \to e^{-i\varphi_i}L_i, \quad \text{and} \quad E_i \to e^{i\varphi_i}E_i, \tag{A.6}$$

where φ_is are defined as

$$\begin{aligned} \varphi_1 &= \left(arg.(\kappa_{12}) + arg.(\kappa_{13}) - arg.(\kappa_{23})\right)/4, \\ \varphi_2 &= \left(arg.(\kappa_{12}) - arg.(\kappa_{13}) + arg.(\kappa_{23})\right)/4, \\ \varphi_3 &= \left(-arg.(\kappa_{12}) + arg.(\kappa_{13}) + arg.(\kappa_{23})\right)/4. \end{aligned} \tag{A.7}$$

Normalizing all elements by κ_{23}, κ is given by

$$\begin{aligned}\kappa &= \kappa_{23}\begin{pmatrix} 0 & r''_1 & r''_2 \\ r''_1 & 0 & 1 \\ r''_2 & 1 & 0 \end{pmatrix}, \\ &= \kappa_{23}\begin{pmatrix} \sqrt{r''_1 r''_2} & 0 & 0 \\ 0 & \sqrt{r''_1/r''_2} & 0 \\ 0 & 0 & \sqrt{r''_2/r''_1} \end{pmatrix}\begin{pmatrix} 0 & 1 & 1 \\ 1 & 0 & 1 \\ 1 & 1 & 0 \end{pmatrix} \\ &\quad\times\begin{pmatrix} \sqrt{r''_1 r''_2} & 0 & 0 \\ 0 & \sqrt{r''_1/r''_2} & 0 \\ 0 & 0 & \sqrt{r''_2/r''_1} \end{pmatrix}, \end{aligned} \tag{A.8}$$

where

$$r''_1 = \frac{\kappa_{12}}{\kappa_{23}}, \quad \text{and} \quad r''_2 = \frac{\kappa_{13}}{\kappa_{23}}. \tag{A.9}$$

By using the notation of (3.8), we can obtain $r''_{1,2}(M_R)$ as

$$\begin{aligned} r''_1(M_R) &= r''_1(m_Z)\sqrt{\frac{I_e}{I_\tau}}, \\ r''_2(M_R) &= r''_2(m_Z)\sqrt{\frac{I_e}{I_\mu}}. \end{aligned} \tag{A.10}$$

Then, $\kappa(M_R)$ is given by

$$\begin{aligned}\kappa(M_R) &= \frac{\kappa_{23}(M_R)}{\kappa_{23}(m_Z)}\sqrt{\frac{I_\tau}{I_\mu}}\begin{pmatrix} \sqrt{I_e/I_\tau} & 0 & 0 \\ 0 & \sqrt{I_\mu/I_\tau}\,0 & \\ 0 & 0 & 1 \end{pmatrix}\kappa(m_Z) \\ &\quad\times\begin{pmatrix} \sqrt{I_e/I_\tau} & 0 & 0 \\ 0 & \sqrt{I_\mu/I_\tau}\,0 & \\ 0 & 0 & 1 \end{pmatrix}. \end{aligned} \tag{A.11}$$

Equations (A.5) and (A.11) show that the energy-scale dependence of the MNS matrix can be estimated by $\sqrt{I_e/I_\tau}$ and $\sqrt{I_\mu/I_\tau}$ even in the cases of $\kappa_{33} = 0$ or $\kappa_{11} = \kappa_{22} = \kappa_{33} = 0$. In general, quantum corrections of the MNS matrix can be estimated by only $n_g - 1$ degrees of freedom [21]. This is easily understood as follows. The RGE of κ ((3.1)) is separated into two parts, which are the lepton-flavor independent terms and the lepton-flavor dependent terms The energy-scale dependences of the mixing angles of κ are determined by the flavor-dependent corrections from $y^{\rm e}$. Since $y^{\rm e}$ has n_g degrees of freedom, expect for the over-all factor, $n_g - 1$ degrees of freedom determine the energy-scale dependence of the MNS matrix, as shown in (3.9), (A.5) and (A.11).

B Approximation of the renormalization corrections

We show the approximation of $\sqrt{I_i/I_\tau}$. Although we do not use this approximation in our numerical analyses, it is useful for a rough estimate of quantum corrections of κ.

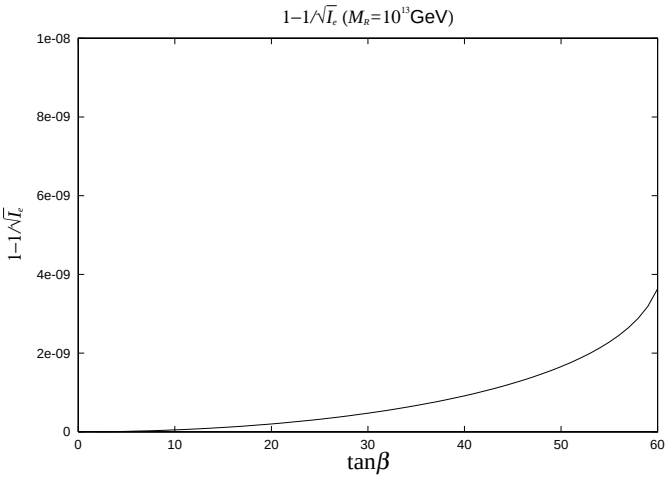

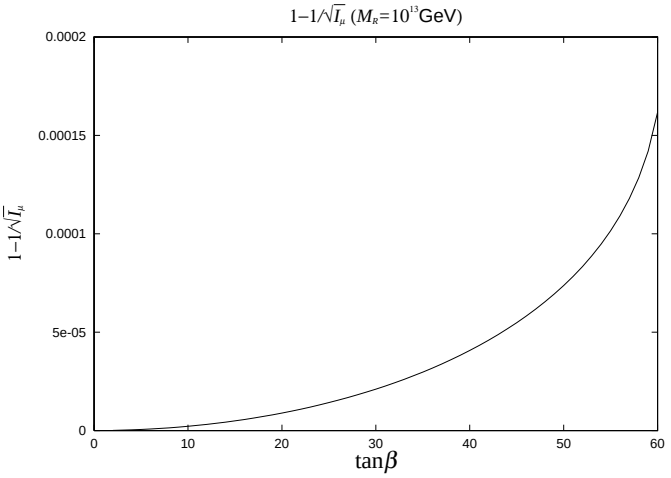

Fig. 8a,b. $\tan\beta$ dependences of (B.1)

At first, let us estimate the values of

$$\frac{\sqrt{I_{e,\mu}/I_\tau}-\sqrt{1/I_\tau}}{\sqrt{I_{e,\mu}/I_\tau}}=1-\frac{1}{\sqrt{I_{e,\mu}}}\,. \tag{B.1}$$

The magnitudes of (B.1) are estimated to be

$$0<1-\frac{1}{\sqrt{I_e}}\ll 10^{-8}\quad\text{and}\quad 0<1-\frac{1}{\sqrt{I_\mu}}\ll 10^{-3} \tag{B.2}$$

in the region of $2\leq\tan\beta\leq 60$ from the numerical analysis shown in Figure 8. Thus, the approximation

$$\sqrt{\frac{I_{e,\mu}}{I_\tau}}\simeq\frac{1}{\sqrt{I_\tau}} \tag{B.3}$$

is valid with good accuracy. If we neglect the energy-scale dependence of y_τ, the value of (B.3) is given by

$$\ln\left(\frac{1}{\sqrt{I_\tau}}\right)=\frac{1}{8\pi^2}\left(\frac{m_\tau}{v}\right)^2\left(\tan\beta^2+1\right)\ln\left(\frac{m_Z}{M_R}\right) \tag{B.4}$$

from (3.8), where m_τ is the mass of τ-lepton and $v^2=\langle\phi_{\rm d}^2\rangle+\langle\phi_{\rm u}^2\rangle$. We define the faction of

$$Err(\tan\beta,M_R)=1-\sqrt{I_\tau} \tag{B.5}$$

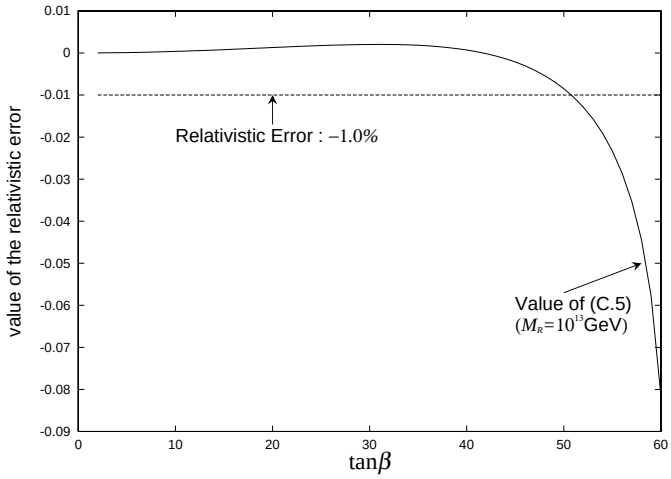

Fig. 9. $\tan\beta$ dependence of (B.6)

$$\times\left(\frac{m_Z}{M_R}\right)\frac{1}{8\pi^2}\left(\frac{m_\tau}{v}\right)^2\left(\tan\beta^2+1\right)$$

to check the accuracy of (B.4). The $\tan\beta$ dependence of $|Err|$ is shown in Figure 9 with $M_R=10^{13}$ GeV. In the region $2\leq\tan\beta\leq 50$, the error of (B.4) is less than 1%. Even in the region $50\leq\tan\beta\leq 60$, where the energy scale dependence of y_τ cannot be neglected, $|Err|$ is less than 10%.

If M_R is smaller than 10^{13} GeV, the approximation of (B.4) becomes more accurate because the Yukawa couplings of the charged-leptons are enhanced in the high energy scale.

Note added:

After we submitted this work for publication, we received a paper hep-ph/9906470 [25] by R. Barbieri, G.G. Ross and A. Strumia. They have shown that the MNS matrix is not spoiled by quantum corrections in some types of neutrino mass hierarchy. All their findings are understood as special cases of our results.

References

1. Homestake Collaboration, B.T. Cleveland et al., Nucl. Phys.(Proc. Suppl.) B **38**, 47 (1995); Kamiokande Collaboration, Y. Suzuki, Nucl. Phys. (Proc. Suppl.) B **38**, 54 (1995); GALLEX Collaboration, P. Anselmann et al., Phys. Lett. B **357**, 237 (1995); SAGE Collaboration, J.N. Abdurashitov et al., Phys. Lett. B **328**, 234 (1994); Super-Kamiokande Collaboration, Phys. Pev. Lett. **82**, 1810 (1999); hep-ex/9812011; hep-ex/9903034
2. Kamiokande Collaboration, K.S. Hirata et al., Phys. Lett. B **205**, 416 (1988); ibid. B **280**, 146 (1992); Y. Fukuda et al., Phys. Lett. B **335**, 237 (1994); IMB Collaboration, D. Casper et al., Phys. Pev. Lett. **66**, 2561 (1991); R. Becker-Szendy et al., Phys. Rev. D **46**, 3720 (1992); SOUDAN2 Collaboration, T. Kafka, Nucl. Phys. (Proc. Suppl.) B **35**, 427 (1994); M.C. Goodman, ibid. **38**, (1995) 337; W.W.M. Allison et al., Phys. Lett. B **391**, 491 (1997); Phys. Lett. B **449**, 137 (1999)

3. Y. Totsuka, invited talk at the 18th International Symposium on Lepton-Photon Interaction, July 28 - August 1, 1997 Hamburg; Super-Kamiokande Collaboration, Phys. Pev. Lett. **81**, 1562 (1998); Phys. Pev. Lett. **82**, 2644 (1999); hep-ex/9903047
4. The CHOOZ Collaboration, Phys. Lett. B **420**, 397 (1998)
5. Z.Maki, M.Nakagawa, S.Sakata, Prog. Theor. Phys. **28**, 870 (1962)
6. See, for example, M. Bando, Izawa Ken-Iti, T. Takahashi, Prog. Theor. Phys. **92**, 1137 (1994); M. Schmaltz, Phys. Rev. D **52**, 1643 (1995); Y. Achiman, T. Greiner, Nucl. Phys. B **443**, 3 (1995); G.K. Leontaris, S. Lola, G.G. Ross, Nucl. Phys. B **454**, 25 (1995); M. Tanimoto, Phys. Lett. B **360**, 41 (1995); G.K. Leontaris, S. Lola, hep-ph/9510340; Mar Bastero-Gil, B. Brahmachari, Nucl. Phys. B **482**, 39 (1996); G. Lazarides, Q. Shafi, N.D. Vlachos, Phys. Lett. B **427**, 53 (1998); M.K. Parida, N. Nimai Singh, Phys. Rev. D **59**, 032002 (1999); B. Brahmachari, R.N. Mohapatra, Phys. Rev. D **58**, 015003 (1998); N. Haba, T. Matsuoka, Prog. Theor. Phys. **99**, 831 (1998); G. Lazarides, hep-ph/9801340, to be published in the proceedings of COSMO-97; C.H. Albright, K.S. Babu, S.M. Barr, Phys. Pev. Lett. **81**, 1167 (1998); G. Lazarides, hep-ph/9802415, Lectures given at 6th BCSPIN Kathmandu Summer School in Physics; B.C. Allanach, Phys. Lett. B **450**, 182 (1999); M. Tanimoto, hep-ph/9807517; N. Haba, Phys. Rev. D **59**, 035011 (1999); J. Ellis, G.K. Leontaris, S. Lola, D.V. Nanopoulos, Eur.Phys.J. C9 389 (1999); S. Lola, G.G. Ross, Nucl. Phys. B **553**, 81 (1999); Y. Nir, Y. Shadmi, JHEP 9905 023 (1999); S. Lola, hep-ph/9903203, Contribution to the 1998 Corfu Summer Institute on Elementary Particle Physics, to appear in JHEP proceedings; K.S. Babu, B. Dutta, R.N. Mohapatra, Phys. Lett. B **458**, 93 (1999); M. Carena, J. Ellis, S. Lola, C.E.M. Wagner, hep-ph/9906362
7. G. Altarelli, F. Feruglio, JHEP 9811 021 (1998)
8. J. Ellis, S. Lola, Phys. Lett. B **458**, 310 (1999)
9. J.A. Casas, J.R. Espinosa, A. Ibarra, I. Navarro, Nucl. Phys. B **556**, 3 (1999) and hep-ph/9905381
10. J.A. Casas, J.R. Espinosa, A. Ibarra, I. Navarro, JHEP 9909 015 (1999)
11. K. Hagiwara, N. Okamura, Nucl. Phys. B **548**, 60 (1999)
12. N. Cabibbo, Phys. Pev. Lett. **10**, 531 (1964); M. Kobayashi, T. Maskawa Prog. Theor. Phys. **49**, 652 (1973)
13. Particle Data Group, The European Physical Journal C **3**, 1 (1998); htt://pdg.lbl.gov
14. L. Wolfenstein. Phys. Pev. Lett. **51**, 1945 (1983)
15. M. Kobayashi, Prog. Theor. Phys. **92**, 287 (1994); ibid **92**, 289 (1994)
16. L. Wolfenstein, Phys. Rev. D **17**, 2369 (1978); S.P. Mikheyev, A.Yu. Smirnov, Yad. Fiz. **42**, 1441 (1985) [Sov.J.Nucl.Phys.**42**, 913 (1986)]; Nuovo Cimento C **9**, 17 (1986)
17. B. Pontecorvo, Zh.Eksp. Teor. Fiz. **53**, 1717 (1967); S.M. Bilenky, B. Pontecorvo, Phys. Rep. **41**, 225 (1978); V. Barger, R.J.N. Phillips, K. Whisnant, Phys. Rev. D **24**, 538 (1981); S.L. Glashow, L.M. Krauss, Phys. Lett. **190B**, 199 (1987)
18. P.H. Chankowski, Z. Pluciennik, Phys. Lett. **316B**, 312 (1993)
19. K.S. Babu, C.N. Leung, J. Pantaleone, Phys. Lett. **319B**, 191 (1993)
20. T. Yanagida, in Proceedings of the Workshop on Unified Theory and Baryon Number in the Universe, ed. O. Sawada, A. Sugamoto (KEK, report 79-18, 1979), p.95; M. Gell-Mann, P. Ramond, S. Slansky, in Supergravity, ed. P. van Nieuwenhuizen, D.Z. Freedman (North-Holland, Amsterdam, 1979), p315; R. Mohapatra, S. Senjanović, Phys. Pev. Lett. **44**, 912 (1980)
21. N. Haba, Y. Matsui, N. Okamura, M. Sugiura, Eur. Phys. J. C10 677 (1999)
22. N. Haba, N. Okamura, M. Sugiura, hep-ph/9810471 to be published in Prog. Theor. Phys. Vol.103 , No.2
23. H. Georgi, S.L. Glashow, hep-ph/9808293
24. L. Baudis, et al., Phys. Pev. Lett. **83**, 41 (1999)
25. R. Barbieri, G.G. Ross, A. Strumia, JHEP 9910 020 (1999)